UNIVERSITY OF VAASA

FACULTY OF TECHNOLOGY

ENERGY ENGINEERING

Antti Savola

FLUID FLOW MODELING INSIDE HEAT COLLECTION PIPES WITH FINITE ELEMENT METHOD

Master's thesis for the degree of Master of Science in Technology submitted for inspection, Vaasa, 20.03.2012

Supervisor	Professor Seppo Niemi (D.Sc.)
Instructor	Jukka Kiijärvi (D.Sc.)

PREFACE AND ACKNOWLEDGEMENTS

This thesis is written for the University of Vaasa and is part of the preparation work for the *Geoenergy Research Project*.

My introduction to geoenergy was when I started to work as a project researcher in the *Geoenergy Research Project* in the University of Vaasa. I started to work on the project in the spring of 2010, and to write my master's thesis in September 2011. During the preparation of the *Geoenergy Research Project* I was able to study the field very closely and also get to know some of the experts and companies working in the field.

The aim of the *Geoenergy Research Project* is to utilize the heat of different stratum layers (e.g. water system, soil, seabed sediment, rock, asphalt) using as effective methods as possible. The aim is to find a working research and development center on the coastline of the University of Vaasa. The center is also meant to be used for multilingual education at international level. The mobile unit enables national research and even international customized research. The energy produced both during the research periods and outside them is meant to be used in the properties of the neighboring areas. (Appendix 1)

I would like to address my special thanks to Mauri Lieskoski who first suggested that I would study fluid flow behavior inside heat collection pipes. Over the past few years Mr. Lieskoski has helped me to find answers and solutions to my many questions about the field of geoenergy engineering. Thanks to my supervisor Professor Seppo Niemi and instructor Jukka Kiijärvi for their support and help during my thesis writing. Professor Seppo Niemi gave many good advices during my studies. Jukka Kiijärvi gave me a lot of important information about modeling and simulation processes.

I would also like to extend a warm gratitude to Development Director Johan Wasberg from Merinova Ltd. Mr. Wasberg has given me a number of good advices during my research work. Thanks also to my supervisor Research Manager Erkki Hiltunen from the University of Vaasa. Thanks also to Johanna Ojaharju for the proofreading.

My greatest thanks go to my lovely wife Jenni. Jenni has been a great support to me during my studies. Together we have been walking on the same road for ten years now and many times I have noticed that Jenni has much more commonsense than me when it comes to engineering applications.

Vaasa, 20.03.2012

Antti Savola

TABLE OF CONTENTS **page**

PREFACE AND ACKNOWLEDGEMENTS 2

SYMBOLS AND ABBREVIATIONS 6

ABSTRACT 13

TIIVISTELMÄ 14

1 INTRODUCTION 15
1.1 Current Situation in the Geoenergy Sector 15
1.2 Aim of the Thesis 16

2 BASICS 18
2.1 Geoenergy 18
2.1.1 The Heat Pump 19
2.1.2 The Energy Source and the Thermal Process in the Ground 21
2.2 Fluid Dynamics and Heat Transfer 23
2.2.1 Fluid Flow 23
2.2.2 Internal Forced Convection 25
2.2.3 Viscosity as a function of the Reynolds Number 26
2.2.4 Heat Transfer in Turbulent Flow 29
2.2.5 Pressure Drop 30

3 COMPUTATIONAL FLUID DYNAMICS 31

4 DIFFERENT MODELING METHODS 38
4.1 The Finite Difference Method 38
4.2 The Finite Volume Method 39
4.3 The Finite Element Analysis and the Finite Element Method 40

5 FLUID FLOW MODELING WITH COMSOL MULTIPHYSICS 42
5.1 Smooth U-Pipe in 2D (Short) 43
5.2 Smooth U-Pipe in 2D (Long) 46

5.3 Finned U-Pipe in 2D (Short) 49
5.4 Finned U-Pipe in 2D (Long) 52
5.5 Example of a Flow Model in a Wide Heat Collection Pipe 55
5.6 A Twisted Tape inside a Smooth Pipe in 3D 57
5.7 Twisted Tape inside a Smooth U-Pipe in 3D 58
5.8 Approximation of Pressure drop and Pumping Power Variations 60

6 DISCUSSION 61

7 CONCLUSIONS 64

8 SUMMARY 66

LIST OF REFERENCES 67

APPENDICES 72
APPENDIX 1: Geoenergy Research Project 72
APPENDIX 2: Heat Equation 73
APPENDIX 3: Moody Diagram 74
APPENDIX 4: Mean Velocity and Mean Temperature 75
APPENDIX 5: Densities and Viscosities of Ethanol-Water Mixtures 76

SYMBOLS AND ABBREVIATIONS

Symbols used

A_c	Cross-sectional area (m^2)
π	Pi
γ	Euler's - Mascheroni constant (0,5772…)
ε	Dissipation rate of turbulence energy
ε/D	Relative roughness
μ	Dynamic viscosity (Pa · s)
η_C	*Carnot* efficiency
λ	Heat conductivity (W/K m)
$\frac{\lambda}{\rho c_v}$	Thermal diffusivity (m^2/s)
ν	Kinematic viscosity (m^2/s)
ρ	Density (kg/m^3)
Φ_{pump}	Pumping power (W)
θ	Angle
ϕ	Angle
C	Heat capacity (J/K)
cos (α)	Function Cosine (adjacent/hypotenuse) of an angle α
cot (α)	Function Cotangent (adjacent/opposite) of an angle α
c_p	Specific heat capacity (J/kg K)
c_v	Specific volumetric heat capacity (J/m^3 K)
D	Diameter of flow section (m)
D_f	Friction coefficient
$\boldsymbol{e}_{...}$	Space-unit-vector direction
f	Friction factor
$\boldsymbol{F}$	External force-vector, e.g. gravity (N)
$\boldsymbol{g}_r$	Gravity constant – vector on the direction r (m/s^2)
$\boldsymbol{g}_\phi$	Gravity constant – vector on the direction ϕ (m/s^2)
$\boldsymbol{g}_\theta$	Gravity constant – vector on the direction θ (m/s^2)
$\boldsymbol{g}_x$	Gravity constant – vector on the direction x (m/s^2)

$\boldsymbol{g}_{\mathrm{y}}$	Gravity constant – vector on the direction y (m/s^2)
$\boldsymbol{g}_{\mathrm{z}}$	Gravity constant – vector on the direction z (m/s^2)
Δh	Specific enthalpy difference (J/kg)
h_{i}	Heat transfer coefficient (W/m^2 K)
ΔH_{vap}	Enthalpy of vaporization (J/kg)
$\boldsymbol{I}$	Unit vector
L	Length of flow section (m)
$\dot{m}$	Mass flow rate (kg/s)
Nu	Nusselt Number
Δp	Pressure drop (Pa)
Pr	Prandtl Number
Q_{H}	Heat rejected from the heat pump (J)
Q_{L}	Heat removed from the heat source (J)
q'	Thermal power per unit length (heat flux) (W/m)
q''	Thermal power per unit area (heat flux density) (W/m^2)
$\boldsymbol{q}''$	Heat flux density – vector (W/m^2)
q''_{conv}	Heat transfer by convection (W/m^2)
r	Radius (m)
R	Pipe radius (m)
Re	Reynolds Number
s	Independent parameter (in step-function)
sin (α)	Function Sine (opposite/hypotenuse) of an angle α
$\frac{\partial T}{\partial t}$	Time-dependent change in temperature (K/s)
$\frac{\partial T}{\partial x}$	Temperature gradient (K/m)
ΔT	Temperature difference (K)
T_{c}	Condensation temperature (K)
$T_{\mathrm{distribution}}$	Heat distribution temperature (K)
T_{e}	Evaporation temperature (K)
$\mathcal{T}_{\mathrm{m}}$	Mean temperature (K)
T_{s}	Surface temperature of the pipe (K)
T_{source}	Heat source's temperature (K)
T_{∞}	Temperature of the fluid sufficiently far from the surface (K)

t	Time (s)
ΔU	Internal energy (J)
U_mean	Mean velocity inside step-function (m/s)
$\boldsymbol{V}$	Averaged velocity vector (m/s)
v	Flow velocity (m/s)
$\boldsymbol{v}$	Velocity vector (m/s)
$\boldsymbol{v}_{\mathrm{r}}$	Velocity vector – on the direction r (m/s)
$\boldsymbol{v}_{\phi}$	Velocity vector – on the direction ϕ (m/s)
$\boldsymbol{v}_{\theta}$	Velocity vector – on the direction θ (m/s)
$\boldsymbol{v}_{\mathrm{x}}$	Velocity vector – on the direction x (m/s)
$\boldsymbol{v}_{\mathrm{y}}$	Velocity vector – on the direction y (m/s)
$\boldsymbol{v}_{\mathrm{z}}$	Velocity vector – on the direction z (m/s)
$\boldsymbol{v}'$	Averaged outer vector field (m/s)
$\mathcal{V}_{\mathrm{m}}$	Mean velocity (m/s)
$\dot{V}$	Volumetric flow rate of the fluid flow (m^3/s)
$W_{\mathrm{net,in}}$	Work input (J)
x	Independent variable (in elliptical paraboloid equation)
y	Independent variable (in elliptical paraboloid equation)
$\boldsymbol{\nabla}$	Nabla operator (vector – operator)
∇^2	Laplace operator
$\otimes$	Outer vector product
$()^T$	Transpose of a matrix ()

Abbreviations used

BD	Boundary Conditions
CFD	Computational Fluid Dynamics
COP_{HP}	Coefficient of Performance of heat pump (heating mode)
DAE	Differential Algebraic Equations
FDM	Finite Difference Method
FEA	Finite Element Analysis
FEM	Finite Element Method
FVM	Finite Volume Method
GSHP	Ground Source Heat Pump
IBVP	Initial Boundary Value Problem
IC	Initial Conditions
ODE	Ordinary Differential Equations
PDE	Partial Differential Equations
PVC	Polyvinyl Chloride
RANS	Reynolds Average Navier-Stokes equations
in situ	in position *(lat.)*

FIGURES **page**

Figure 1. Temperature Profiles from the Ground on Different Periods of the Year 18
Figure 2. The Heat Pump Operation Cycle 20
Figure 3. Kinematic Viscosity as a Function of Temperature 27
Figure 4. Kinematic Viscosity as a Function of the Reynolds Number with Diameter 1 28
Figure 5. Kinematic Viscosity as a Function of the Reynolds Number with Diameter 2 28
Figure 6. Finned (a), Roughened (b) and Grooved (c) Inner Surfaces of the Pipe 29
Figure 7. Figure 7. FEM Solutions for 2D- Magnetostatic Configuration (Left) and Meshing (Middle) and Visualization of how a Car Deforms in an Asymmetrical Crash (Right) 40
Figure 8. 3D-Mesh for Axially Placed Fins inside the Pipe 41
Figure 9. Smooth and Axial-Finned inside Profile 42
Figure 10. The Velocity Profile of a Smooth-Short U-Pipe 43
Figure 11. The Velocity Profile of a Smooth-Short U-Pipe (Zoomed) 44
Figure 12. The Pressure Profile of a Smooth-Short U-Pipe 44
Figure 13. The Pressure Profile of a Smooth-Short U-Pipe (Zoomed) 45
Figure 14. Velocity Profile Variations in a Smooth-Short U-Pipe 45
Figure 15. The Velocity Profile of a Smooth-Long U-Pipe 47
Figure 16. The Pressure Profile of a Smooth-Long U-Pipe 47
Figure 17. Velocity Profile Variations in a Smooth-Long U-Pipe 48
Figure 18. The Velocity Profile of a Finned-Short U-Pipe 49
Figure 19. The Velocity Profile of the Finned-Short U-Pipe (Zoomed) 50
Figure 20. The Pressure Profile of a Finned-Short U-Pipe 50
Figure 21. The Pressure Profile of a Finned-Short U-Pipe (Zoomed) 51
Figure 22. Velocity Profile Variations in a Finned Pipe 51
Figure 23. The Velocity Profile of a Finned-Long U-Pipe 53
Figure 24. The Pressure Profile of a Finned-Long U-Pipe 53
Figure 25. Velocity Profile Variations in a Long Finned Pipe 54
Figure 26. The Velocity Profile of a Smooth U-Pipe 55
Figure 27. Velocity Profile Variations in a Smooth Pipe 55
Figure 28. The Velocity Profile of a Finned U-Pipe 56
Figure 29. Velocity Profile Variations in a Finned Pipe 56
Figure 30. A Twisted Tape inside a Smooth Pipe 57
Figure 31. Velocity and Pressure Profiles in a Pipe with Twisted Tape Inserts 58
Figure 32. A Twisted Tape inside a Smooth U-Pipe 59

Figure 33. Velocity and Pressure Profiles in a U-Pipe with Twisted Tape Inserts 59

Figure 34. The Range of Pressure Drop and Pumping Power in Smooth and Finned Pipes and a Pipe where a Twisted Tape is Placed in the middle of the Pipe 60

Figure 35. The Schematic of an inner fin structure 62

Figure 36. Evaporation (left) and Condensation (right) Heat Transfer Coefficient vs. Heat Flux 62

Figure 37. Geometries of a Peripherally-Cut Twisted Tape (PT) and a Typical Twisted Tape 63

TABLES **page**

Table 1. Some Properties of Different Energy Sources 19
Table 2. Specific Heat Capacities per Meter 22

UNIVERSITY OF VAASA
Faculty of Technology
Author: Antti Savola
Topic of the Thesis: Fluid flow modeling inside heat collection pipes with finite element method
Supervisor: Professor Seppo Niemi (D.Sc.)
Instructor: Jukka Kiijärvi (D.Sc.)
Degree: Master of Science in Technology
Degree Programme: Degree Programme in Electrical and Energy Engineering
Major of Subject: Energy Engineering
Year of Entering the University: 2006
Year of Completing the Thesis: 2012 **Pages**: 76

ABSTRACT:

Builders and heat pump and pipe manufactures have faced new challenges as the demand on efficiency has become greater in the geoenergy sector. One method that can be used for increasing the heat transfer capacity in the heat collection systems is to use twisted tape or axially placed fins inside heat collection pipes. These inner structure modifications increase turbulent flow behavior which increases the heat transfer effect by force of convection.

The aim of this thesis was to model fluid flow behavior inside the heat collection pipes with the finite element method. The most important properties which need to be taken into account in order the heat collection fluid flow to be rather turbulent than laminar, are analyzed. The analysis consists of modeling with COMSOL Multiphysics. COMSOL Multiphysics is a finite element method - based on modeling and simulation software.

In this thesis flow behavior inside heat collection pipes with different inner surface structures was modeled. The aim was to find out what kind of flow environment would turn the flow from laminar to turbulent inside the heat collection pipes. Also how the pressure drop and pumping power vary when the inner profile of the heat collection pipe changes is examined. The models that have been built are meant to be mainly indicative. The aim of this thesis was not to design a completely new pipe profile. The aim of this thesis was to demonstrate how turbulent flow behavior in the heat collection pipes of a ground source heat pump system can be achieved. COMSOL models showed that a minor inner surface modification increases turbulence inside the heat collection pipes. The models and results discussed in this thesis are well known and very common in heat recovery engineering solutions, but they have not been discussed before in the field of ground source heat pump systems and heat collection pipes.

KEYWORDS: heat collection pipe, fluid flow, heat transfer by convection, computational fluid dynamics, finite element method

VAASAN YLIOPISTO
Teknillinen tiedekunta
Tekijä: Antti Savola
Diplomityön nimi: Virtauksen mallintaminen lämmönkeräysputkistoissa elementtimenetelmällä
Valvojan nimi: Professori Seppo Niemi (TkT)
Ohjaajan nimi: Jukka Kiijärvi (TkT)
Tutkinto: Diplomi-insinööri
Koulutusohjelma: Sähkö- ja Energiatekniikan koulutusohjelma

Suunta: Energiatekniikka
Opintojen aloitusvuosi: 2006
Diplomityön valmistumisvuosi: 2012 **Sivumäärä**: 76

TIIVISTELMÄ:

Vaatimukset geoenergiajärjestelmien tehokkuuden parantamisesta ovat tuoneet uusia haasteita niin rakentajille, lämpöpumppuvalmistajille kuin putkistovalmistajillekin. Käyttämällä kierre- tai evärakenteita lämmönkeräysputkistojen sisällä voidaan nestevirtauksen turbulenttisuutta nostaa ja tätä hyödyntäen lisätä konvektiivistä lämmönsiirtokapasiteettia.

Tämän diplomityön tarkoituksena oli ensisijaisesti mallintaa elementtimenetelmällä virtauksen käyttäytymistä lämmönkeräysputkistoissa. Tässä diplomityössä tutkitaan, mitkä tekijät ja ominaisuudet on otettava huomioon, jotta lämmönkeräysnesteen virtaus on enemmän turbulenttista kuin laminaarista. Tarkastelut suoritettiin elementtimenetelmään perustuvalla COMSOL Multiphysics-mallinnusohjelmalla.

Tässä diplomityössä mallinnettiin virtauksen käyttäytymistä lämmönkeräysputkistoissa erilaisilla putken sisäprofiileilla. Tarkoitus oli selvittää, minkälainen ympäristö virtauksella tulisi olla, jotta virtaus muuttuisi laminaarisesta turbulenttiseksi. Lisäksi selvitettiin, millä tavoin painehäviöt sekä pumppaustehot muuttuvat, kun lämmönkeräysputkiston sisäprofiili muuttuu. Rakennetut mallit ovat pääsääntöisesti suuntaa antavia. Tämän diplomityön tarkoituksena ei ollut suunnitella täysin uutta putkimallia. Tarkoituksena oli osoittaa kuinka maalämpöjärjestelmien lämmönkeräysputkistojen nestevirtaus saadaan turbulenttiseksi. COMSOL mallinnukset osoittivat, että pienillä sisäprofiilin muutoksilla saadaan muutettua putkivirtausta laminaarisesta turbulenttiseksi. Mallit ja tulokset tässä työssä ovat melko tuttuja lämmöntalteenottoratkaisuista, mutta eivät maalämpöpumppuratkaisujen lämmönkeräysputkistoissa.

AVAINSANAT: lämmönkeräysputki, nestevirtaus, konvektiivinen lämmönsiirto, numeerinen virtauslaskenta, elementtimenetelmä

1 INTRODUCTION

1.1 Current Situation in the Geoenergy Sector

Geoenergy has been used worldwide for several decades, in Finland slightly more than 30 years. The development has been relatively steady, but during the last ten years there has been exponential growth in the use of primary energy produced by ground source heat pumps (SULPU ry 2010). Nevertheless, still today faults and problems come up quite often. These problems are such as heat collection circuit design problems as well as heat pump malfunctions. Thermal power per unit length from the ground (soil, rock etc.) can be determined relatively accurately with the present-day technology. However, more development and research work would be necessary in order to manage the methods and techniques more precisely.

The use of geoenergy in single-family-houses or in larger buildings requires the following issues to be determined: the energy demand on the living area, a suitable ground source heat pump to reply to the energy demand, great enough fluid flow in the heat collection pipes and great enough energy content from the ground. The first two are the easiest issues to be determined, and the last two are the most difficult issues to be determined.

When the geoenergy systems are built, rules-of-thumb methods are often used, especially when dimensioning the energy collection capacity of the heat collection pipe and the heat collection fluid. In many cases these rules have come from a long-time empirical knowledge. This is agreeable, but without proper understanding of the background of the theories these designed systems will not work optimally. Secondary working fluid (heat transfer fluid inside the heat collection pipes) has a major influence on the functionality of the whole geoenergy system. Many studies show that a poor distribution of refrigerant inside the heat pump causes shortening in the running cycle of the heat pump.

This causes regular repayment periods and malfunctions in the heat pump itself. In many cases the poor distribution of refrigerant is caused by incorrectly dimensioned fluid flow in the heat collection pipes. The evaporator of the heat pump will not evaporate the refrigerant properly (and this causes poor distribution of the refrigerant) if the heat collection fluid does not contain enough energy.

In general, the designers are aware that the fluid flow should be turbulent to guarantee as effective heat transfer by convection as possible. However, in many cases, the knowledge of the required qualities of turbulent fluid flow and their role in the functionality of the whole geoenergy system is poor. Heat collection fluid's density (ρ), specific heat capacity (c_p), convection heat transfer coefficient (h_i), heat conductivity (λ), dynamic viscosity (μ), mass flow rate ($\dot{m}$), flow velocity (v), and chemical composition need to be optimized for every single case individually. Also the inner profile of the pipe, relative roughness (ε/D), friction factor (f), friction coefficient (D_f), pressure drop ($\Delta\mathrm{p}$) and pumping power need to be take into consideration in every case.

1.2 Aim of the Thesis

This thesis outlines how the fluid has to flow inside the pipe in order the heat transfer to be as effective as possible. Here was also examined how pressure drop and pumping power vary when the inner profile of the heat collection pipe is changed. The aim of this thesis was not to design a completely new pipe profile or to present new results, because the topic and the results of this thesis are already well known e.g. from the heat recovery systems where twisted inner structures inside the pipe are used. The aim of this thesis was to demonstrate how turbulent flow behavior in heat collection pipes of ground source heat pump system can be achieved. The modeling was done from the point of view of the fluid flow behavior, not from the point of view of the heat transfer behavior. Reason for this was lack of time and also the fact that the modeling work was a lot easier without the time-dependent heat transfer by convection-modeling.

However, modeling just the fluid flow behavior can show quite well when the heat transfer capacity turns better or worse. When the fluid flow is fully turbulent, the heat transfer by convection is efficient. Here every flow area with different temperature is mixed properly and the convection effect is as good as possible. If the fluid flow is fully laminar, the heat transfer cannot take place by the convection in an efficient way. The rule of thumb in the requirements of the turbulent flow behavior is that the Reynolds Number needs to be high enough, approximately 10 000 or more (the Reynolds Number is dimensionless value which tells if the flow is laminar or turbulent or between them). However, this will not guarantee a fully developed turbulent flow just alone, because in very specific circumstances the fluid flow might be laminar even if the Reynolds Number is as high as 40 000.

The above mentioned issues are well known in the field of heat recovery systems (engine technology), but not in the field of heat collection pipes of ground source heat pump systems. The target audience of this thesis is the heat collection pipe designers. In this thesis the flow behavior inside the heat collection pipes with different inner surface structures of the pipe was modeled. The modeling method was the finite element method. The aim was to find out what kind of flow environment would change the flow from laminar to turbulent inside the heat collection pipes. The models that were built are meant to be mainly indicative.

2 BASICS

2.1 Geoenergy

Geoenergy is renewable energy from radiation from the sun which is stored in the upper layers of the ground. Traditional energy sources in geoenergy applications are: water system, soil and bedrock. Less used sources are seabed sediment and asphalt. The properties of soil and seabed sediment are almost identical, except the higher temperature of the seabed. The temperature of the seabed sediment can at its best be from 4 to 5 °C higher than that of the bedrock. The seabed sediment is relatively new energy source and its first applications were taken in use at the Vaasa Housing Fair 2008 (seabed sediment applications are developed in Vaasa). Installation methods used are basically horizontal heat collection pipe loops (water system, soil, seabed sediment and asphalt) or vertical heat collection energy wells (bedrock). Figure 1 and Table 1 show the temperature profiles and properties of the ground.

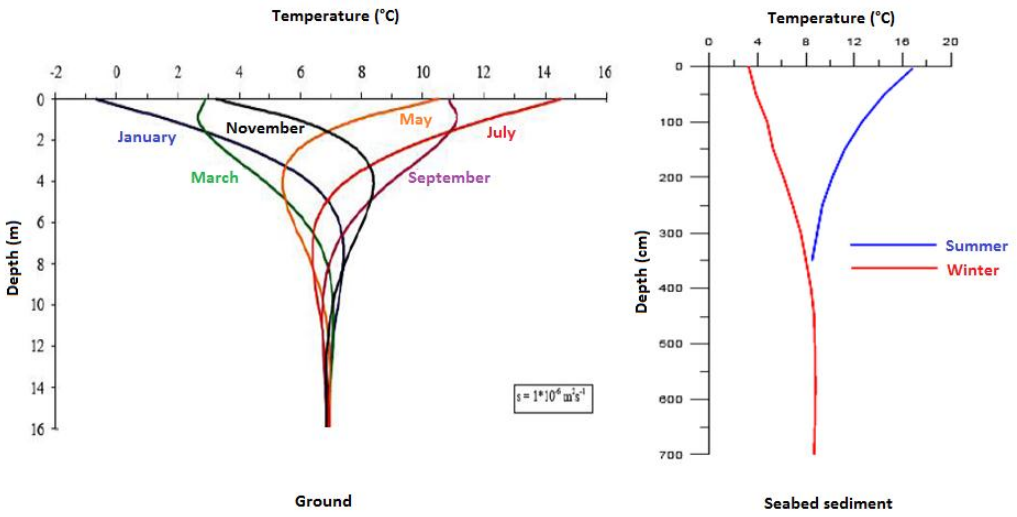

Figure 1. Temperature Profiles from the Ground on Different Periods of the Year (left Leppäharju 2008: 7; right Reinikainen 2009)

Table 1. Some Properties of Different Energy Sources (Pitkäranta 2009: 22; Mateve Ltd. customer magazine 1/2008; GTK 2009; ICAX 2009; Qinwu & Mansour 2009: 494)

Soil material		Heat conductivity	Specific heat capacity	Temperature
Bedrock		3 W/K m	0,75 kJ/Kg K	7-8 °C (at 100 m:n depth)
Soil	dry clay	1,1 W/K m	0,88 kJ/Kg K	7-8 °C (at 8-10 m:n depth)
	wet clay	1,7 W/K m		
	dry sand	0,76 W/K m		
	wet sand	2,5 W/K m		
Water system		0,6 W/K m	4,19 kJ/Kg K	2-4 °C (at the bottom)
Asphalt		2,88 W/K m	0,88–0,92 kJ/Kg K	several tens of degrees

From Figure 1 it can be noticed that the temperature stays quite stationary after 7 meters.

2.1.1 The Heat Pump

Unlike geothermal energy, geoenergy is low temperature heat energy and needs to be used with heat pumps (geothermal energy is from the inner core of the globe and it is high temperature heat energy). The ground source heat pump (GSHP) draws energy from the source and transfers this energy and the mechanical energy (electrical energy) used to operate the vapor-compression cycle so that it can be used for heating. So, the heat pump transforms thermal energy in low temperature into thermal energy at high temperature using mechanical energy. Coefficient of performance (COP) describes the ratio of produced energy in relation to the energy required (Equation 1).

$$\mathrm{COP_{HP}} = \frac{Q_{\mathrm{H}}}{W_{\mathrm{net,in}}} \tag{1}$$

Where is Q_{H} is heat rejected from the heat pump and $W_{\mathrm{net,in}}$ is work input (mechanical energy). If GSHP's $\mathrm{COP_{HP}}$ value is 3, the produced total energy (Q_{H}) consist about one part of electrical energy ($W_{\mathrm{net,in}}$) and two parts of renewable geoenergy (Q_{L}).

In ideal circumstances the heat pump takes heat from the source in a temperature as high as possible and emits it in a temperature as low as possible (Saksi 2008: 4). The situation is ideal when the temperature of the heat source (T_{source}) is the same as the evaporating temperature (T_{e}) inside the heat pump and the heat distribution temperature ($T_{\text{distribution}}$) is the same as the condensation temperature (T_{c}). GSHP's working principle is the following (Figure 2): the refrigerant fluid requires energy to evaporate. That energy is taken from the ground using the heat collection pipes and heat collection fluid, and then transferred to the evaporator of the heat pump. After that the refrigerant vapor is compressed into higher pressure and temperature by using the compressor. The high pressure hot steam is transferred into the condenser where it condenses back into liquid, releasing heat energy for the heating purpose. Condensed refrigerant is returned into its normal state trough an expansion valve. Figure 2 describes only a basic working cycle of the heat pump and it does not tell whether there is an electric heating element (resistance) or extra heat exchanger to remove superheated refrigerant for the water heating purpose and beyond.

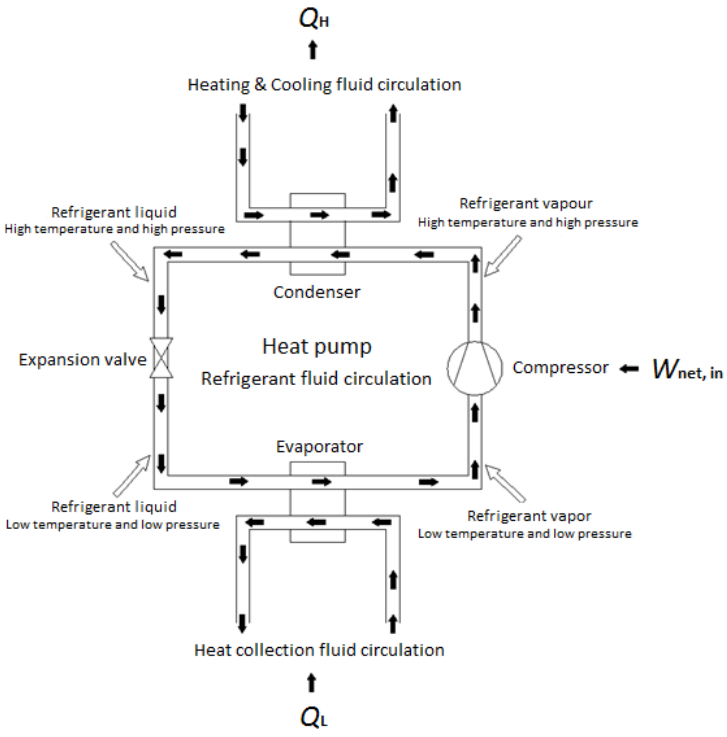

Figure 2. The Heat Pump Operation Cycle

2.1.2 The Energy Source and the Thermal Process in the Ground

Heat transfer can take place in three different ways under the ground: by conduction, convection and radiation (Gupta & Roy 2006; Çengel 2003). Heat transfer under the ground is governed by three dimensional spherical coordinates. In case of heat collection pipes the heat transfer is governed by cylindrical coordinates with the *Heat Equation* (Equation 2).

$$\frac{\partial T}{\partial t} = \frac{1}{r}\frac{\partial T}{\partial r}\left(\frac{\lambda}{\rho c_{\mathrm{v}}} r \frac{\partial T}{\partial r}\right) + \frac{1}{r^2}\frac{\partial T}{\partial \phi}\left(\frac{\lambda}{\rho c_{\mathrm{v}}}\frac{\partial T}{\partial \phi}\right) + \frac{\partial T}{\partial z}\left(\frac{\lambda}{\rho c_{\mathrm{v}}}\frac{\partial T}{\partial z}\right) \quad (2)$$

Where: $\frac{\partial T}{\partial t}$ is time-dependent change in temperature, r is radius, ϕ is angle, z is the direction of the coordinate axel in the cylindrical coordinate system, $\frac{\partial T}{\partial r}$ is temperature change on the direction of r, $\frac{\partial T}{\partial \phi}$ is temperature change on the direction of ϕ and $\frac{\partial T}{\partial z}$ is temperature change on the direction of z. Equation 2 is controlled by thermal diffusivity ($\lambda/\rho c_{\mathrm{v}}$), which is the ratio of the heat conducted and stored and it describes how fast heat diffuses through a material. There the specific volumetric heat capacity (c_{v}) is used instead of specific heat capacity (c_{p}) (Leppäharju 2008: 5). The *heat equation* is derived on Appendix 2. In stationary conditions, the rejected heat from the ground (thermal power per unit area) can be expressed with Equation 3 (*Fourier's first Law*).

$$q'' = -\lambda \frac{\partial T}{\partial x} \quad (3)$$

Where: q'' is heat flux density, λ is thermal conductivity, and $\frac{\partial T}{\partial x}$ is temperature gradient. Groundwater flow has a major influence on the thermal properties of the ground (Gehlin 1998, 2002; Acuña 2010). Water has quite a low heat conductivity value (0,6 W/m K), so water resists heat transfer well. When there is groundwater flow which causes natural convection in the water that surrounds the heat collection pipes, thermal conductivity will be much greater and due to this the heat transfer effect will be much greater.

The effect of the groundwater flow decreases when distance from the heat collection pipe grows, but even a distance of half a meter may result in significant changes in the heat transfer capacity (Gehlin 2002). Normally, water is surrounding heat collection pipes inside vertical borehole on the bedrock, and in this case the effects are even greater. Groundwater flow effects apply in every ground-type.

Thus, the qualities that most affect the receivable energy from the ground are thermal conductivity and thermal resistance (Gehlin 1998, 2002; Leppäharju 2008: 63). This comes up also in the *Fourier's First Law* (Equation 3). The specific heat capacity of the ground has a major impact on the energy content under the ground, but it will not have such a great impact on the heat flux itself. When the heat conductivity of the ground increases, the effect of the rejected heat from the ground decreases. (Leppäharju 2008: 56-57). This is due to the greater thermal power per unit area: temperatures nearby borehole will decrease less. Lower thermal resistance (or higher thermal conductivity) means that a smaller difference in temperature is required between the bedrock and the heat carrier with a given heating power (Gehlin & Nordell 1998). Specific heat capacities per meter are reviewed on Table 2.

Table 2. Specific Heat Capacities per Meter (Ochsner 2008: 50; Dimplex 2008: 76)

Ground type	Heat capacity (W/m)
Dry sand	< 25 W/m
Wet sand	65-80 W/m
Groundwater flow in the sand	80-100 W/m
Dry clay	35-50 W/m
Bedrock (granite)	65-85 W/m

2.2 Fluid Dynamics and Heat Transfer

2.2.1 Fluid Flow

Fluid flow is laminar at low velocities but turns turbulent as the velocity increases beyond the critical value. Transition from laminar to turbulent occurs within a range of velocity where the flow fluctuates between laminar and turbulent flows before becoming fully turbulent. As mentioned earlier, the secondary fluid flow in geoenergy systems needs to be turbulent flow, because then it has the best heat transfer properties (Çengel 2003).

The Reynolds Number (Re) defines whether the fluid is laminar, transitional or turbulent in the following way (Çengel 2003):

$$\begin{aligned} Re &< 2300 \text{ laminar flow} \\ 2300 \leq Re &\leq 10\,000 \text{ transitional flow} \\ Re &> 10\,000 \text{ turbulent flow} \end{aligned}$$

In literature commonly used definitions are only laminar and turbulent flow, not transitional flow. In some special conditions fluid flow might stay transitional even if the Reynolds Number is as high as 40 000 (Hughes, Brighton 1999). In transitional flow the fluid flow switches between laminar and turbulent randomly (Çengel 2003). The Reynolds Number can be calculated from Equation 4 (Çengel 2003).

$$Re = \overbrace{\frac{\rho \mathcal{V}_\mathrm{m} D}{\mu} = \frac{\mathcal{V}_\mathrm{m} D}{\nu}}^{In\ generally} = \overbrace{\frac{\dot{V} D}{\nu A_\mathrm{c}}}^{Pipe\ flow} \tag{4}$$

Where: ρ is density, $\mathcal{V}_\mathrm{m}$ is mean velocity, D is diameter of the pipe, μ is dynamic viscosity, ν is kinematic viscosity, $\dot{V}$ is volumetric flow rate, and A_c is cross-sectional area of the pipe.

The Nusselt Number represents the ratio of the heat transfer through convection (*Newton's Law of Cooling*) and conduction (*Fourier's first Law*) (Equation 5) (Çengel 2003).

$$Nu = \frac{q''_{\text{conv}}}{q''} = \frac{\overbrace{h_{\text{i}}(T_{\text{s}} - T_{\infty})}^{Newton's\ Law\ of\ Cooling}}{\underbrace{\lambda \frac{\partial T}{\partial x}}_{Fourier's\ first\ Law}} \tag{5}$$

Where: q''_{conv} is heat transfer by convection, q'' is heat flux density, h_{i} is heat transfer coefficient, T_{s} is surface temperature, T_{∞} is temperature sufficient far away from the surface, λ is thermal conductivity, and $\frac{\partial T}{\partial x}$ is temperature gradient. The larger the Nusselt Number is the more effective the convection is. If the Nusselt Number is e.g. 1, the heat transfer is purely produced by conduction (Çengel 2003).

The Prandtl Number represents the ratio of the *molecular diffusivity of momentum* (kinematic viscosity) and *molecular diffusivity of heat* (thermal diffusivity) and it describes how great the relative thickness of the velocity and the thermal boundary layers is (Equation 6) (Çengel 2003).

$$Pr = \frac{molecular\ diffusivity\ of\ momentum}{molecular\ diffusivity\ of\ heat} = \frac{\nu}{\frac{\lambda}{\rho C}} = \frac{\mu}{\rho} * \frac{\rho C}{\lambda} = \frac{\mu C}{\lambda} \tag{6}$$

Where: ν is kinematic viscosity, $\frac{\lambda}{\rho C}$ is thermal diffusivity, and C is heat capacity.

Friction factor should be taken into account when designing heat collection pipes. It can be calculated for turbulent flow on smooth- and rough surfaces with Equations 7 and 8 (Çengel 2003):

$$f = (0{,}790 * \ln Re - 1{,}64)^{-2} \qquad (\textit{smooth}) \tag{7}$$

$$\frac{1}{\sqrt{f}} = -2{,}0 * \log\left(\frac{\varepsilon/D}{3{,}7} + \frac{2{,}51}{Re\sqrt{f}}\right) \qquad (\textit{rough}) \tag{8}$$

Where: f is friction factor, *Re* is the Reynolds Number and ε/D is relative roughness.

From Equation 8 it can be noticed that iteration needs to be used unless equation solver is used. Approximation can be used instead of iteration (Equation 9) (Çengel 2003).

$$\frac{1}{\sqrt{f}} = -1{,}8 * \log\left[\frac{6{,}9}{3{,}7} + \left(\frac{\varepsilon/D}{3{,}7}\right)^{1{,}11}\right] \quad (9)$$

Equation 9 is the base of the *Moody Diagram* (Appendix 3). Unlike external flow, internal flow (internal forced convection) has no free stream. Fluid flow velocity in a pipe changes from zero on the surface to a maximum at the center of the pipe because of the no-slip condition. Therefore it is convenient to work with the mean velocity ($\mathcal{V}_\mathrm{m}$), which remains constant for incompressible flow when cross sectional area of the pipe is constant. The mean velocity ($\mathcal{V}_\mathrm{m}$) and the mean temperature ($\mathcal{T}_\mathrm{m}$) are reviewed in Appendix 4 (Çengel 2003).

2.2.2 Internal Forced Convection

Heat transfer by internal forced convection in geoenergy systems is carried out when secondary fluid is forced to flow by a pump through the heat collection pipe. Generally, convection is heat transfer trough fluid in the presence of bulk fluid motion (fluid dynamics) and it can be either natural or forced. Natural convection forms with the rise of warmer fluid and the fall of the cooler fluid, without any external force. (White 2008; Çengel 2003)

Issues that are affecting the heat transfer rate of the secondary working fluid are: heat collection fluid's density (ρ), specific heat capacity (c_p), convection heat transfer coefficient (h_i), heat conductivity (λ), dynamic viscosity (μ), mass flow rate ($\dot{m}$), flow velocity (v) and chemical composition. Also relative roughness (ε/D), friction factor (f), friction coefficient (D_f), pressure drop ($\Delta\mathrm{p}$) and pumping power affect's on the heat transfer rate. In many planning cases it is not so well known how the properties are affecting to each other and especially how the change of some property will affect the other property.

2.2.3 Viscosity as a function of the Reynolds Number

Viscosity fluctuations have major influences on the Reynolds Number and fluid flow behavior. Here is shown how the mixture qualities of the heat collection fluid fluctuate when some properties (e.g. temperature) change. Reviewed issues are mainly kinematic viscosities as a function of the Reynolds Number with different pipe diameters and volumetric flow rates of the fluid.

Water– ethanol mixtures (normally with the ratio of 70 % - 30 %) are normally used as a secondary working fluid in the heat collection pipes of the GSHP system. The flow rate of secondary working fluid is designed to ensure turbulent flow: this guarantees a low convective heat transfer resistance. However, in some heat transfer fluid mixtures, few degrees temperature drop may result in a significant increase in viscosity and this may result in transition to laminar flow. This causes the heat transfer capacity to decrease (Xu, Spitler 2006: 1).

In Equations 5, 6 and 7 it is seen that all the dimensionless quantities (*Re, Nu, Pr*) depend on the kind of qualities which straightly depend on the temperature variations. So it should be taken into account, that few degrees variations in the temperature of secondary fluid may cause significant changes in the fluid properties such as viscosity, which on the other hand may change the value of the Reynolds Number. Figure 3 shows significant fluctuations on the values of kinematic viscosities when the temperature varies. Calculating method for the kinematic viscosity value is presented in Appendix 5. Mixture concentration is expressed e.g. ν (%50), which is water-ethanol mixture with the ratio of 50 – 50.

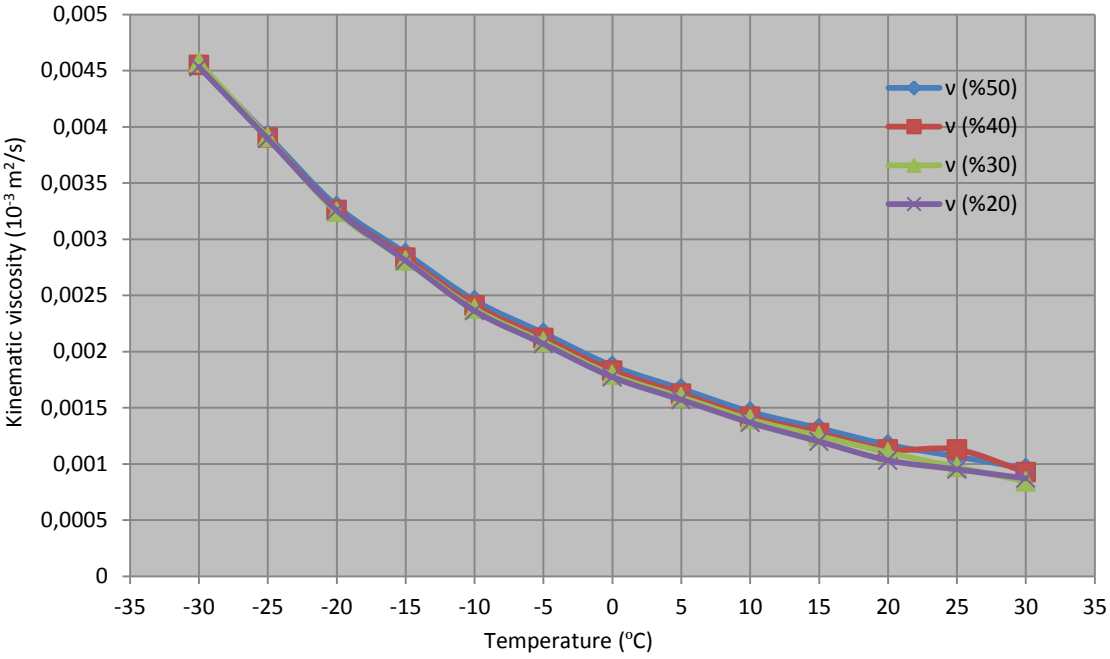

Figure 3. Kinematic Viscosity as a Function of Temperature (the data is from the Altia Corporation)

The same effects that have been noticed in Figure 3 can be also noticed in the case of propylene-glycol-water mixtures. For example, at 20 ºC, the kinematic viscosity of 20% weight concentration propylene-glycol is approximately 2.15 $\mu m^2/s$ and at –5 ºC, the kinematic viscosity increases to 5.56 $\mu m^2/s$. That means, with the same volumetric flow rate, the Reynolds number at –5 ºC is only about 39% of the value at 20 ºC (Xu, Spitler 2006: 1). This causes significant fluctuations for the fluid flow conditions inside the heat collection pipes.

Below are shown the kinematic viscosity variations of the heat collection fluid as a function of the Reynolds Number. The calculating method for the Reynolds Numbers is presented in Appendix 5. In Figure 4 is used 0.6 l/s as a volumetric flow rate and 40 mm as a diameter of the pipe (diameter 1) and in Figure 5 is used 1,0 l/s as a volumetric flow rate and 82 mm as a diameter of the pipe (diameter 2).

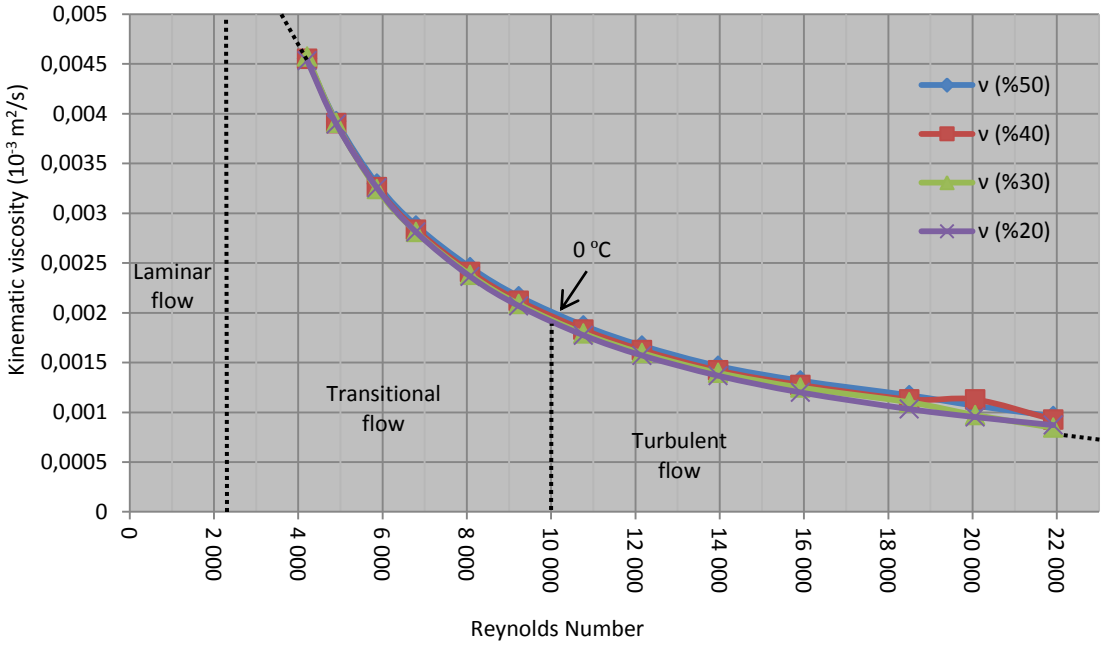

Figure 4. Kinematic Viscosity as a Function of the Reynolds Number with Diameter 1 (part of the data is from the Altia Corporation)

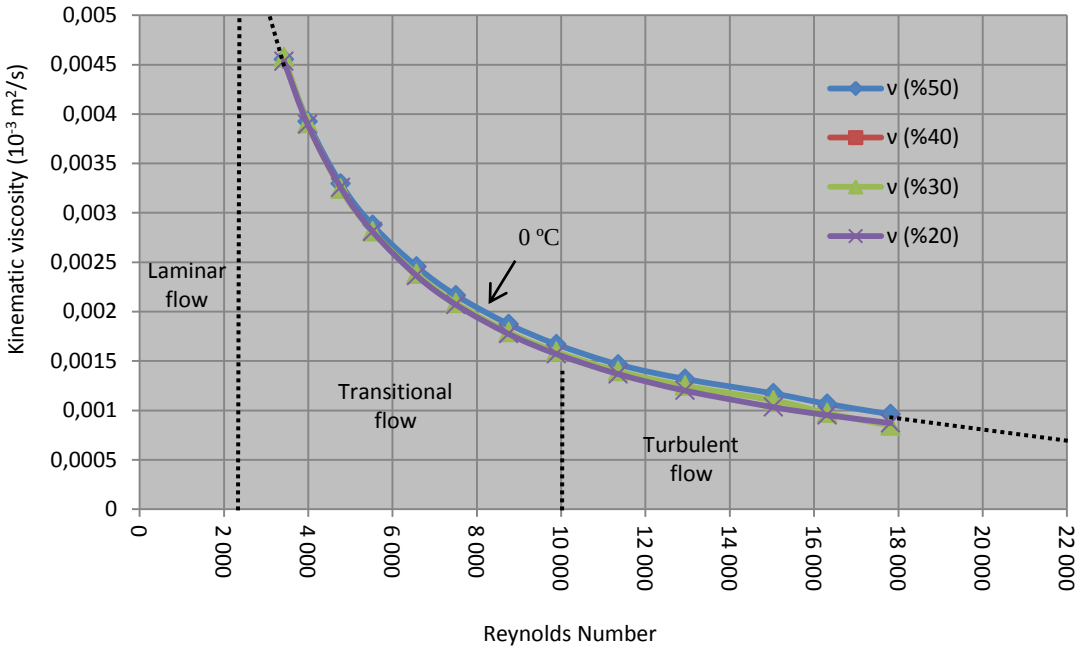

Figure 5. Kinematic Viscosity as a Function of the Reynolds Number with Diameter 2 (part of data is from the Altia Corporation)

Figure 4 shows that the heat collection fluid flow changes to a fully turbulent flow when temperature rises higher than 0 ºC (in case of a smooth pipe). Before that point, the flow conditions change randomly from laminar to turbulent (transitional flow) and this may cause significant decrease in the heat transfer capacity. From Figure 5 it can be noticed that the temperature variations have more influence on the flow conditions when the diameter of the pipe grows.

2.2.4 Heat Transfer in Turbulent Flow

It is important to understand how turbulent fluid flow in the heat collection pipes affects wall shear stress and especially heat transfer rate. Even when the mean flow is steady, the eddying motion in turbulent fluid flow causes significant fluctuations to velocity, temperature, pressure and density. Eddying motion comes from *eddies*, which are group of fluid particles and turbulent fluid flow is characterized by random and rapid fluctuations of those (Çengel 2003). When turbulent fluid flow is full of *eddies*, the fluid is mixed properly and due to this, the turbulent flow brings fluid particles at different temperatures into close contact with each other and the heat transfer comes more effective. The heat transfer rate of turbulent fluid flow in the pipe can be increased by as much as 400 percent (or more) by increasing the inner surface area of the pipe (Çengel 2003). This can be done by roughening or finning the inner surface (Figure 6). Of course doing that will increase the friction factor and power requirement for the circulation pump, so these issues need to be taken into account. Convection heat transfer coefficient can also be increased by inducing pulsating fluid flow by pulse generators or inducing swirl by inserting a twisted tape into the heat collection pipe. (Çengel 2003)

Figure 6. Finned (a), Roughened (b) and Grooved (c) Inner Surfaces of the Pipe. (a and b are from Çengel 2003: 444; c is from Acuña 2010: 61)

2.2.5 Pressure Drop

Pressure drop is directly related to the pumping power requirements that maintain fluid flow in the heat collection pipes. In most of the cases the pressure drop of the laminar flow is expressed, but in practice it is more convenient to express the pressure drop of all types of internal flows and in all conditions (laminar, transitional and turbulent flows, circular and non-circular pipes, smooth and rough surfaces) with Equation 10. (Çengel 2003)

$$\Delta p = f \frac{L}{D} \frac{\rho \mathcal{V}_{\mathrm{m}}{}^{2}}{2} \tag{10}$$

Where: Δp is pressure difference, f is friction factor, L length of the flow section, D is diameter of the flow section, ρ is density, and $\mathcal{V}_{\mathrm{m}}$ is mean velocity. Once the pressure drop is determined, required pumping power can be determined with Equation 11. (Çengel 2003)

$$\Phi_{\mathrm{pump}} = \dot{V} \Delta p \tag{11}$$

Where: Φ_{pump} is pumping power and $\dot{V}$ is volumetric flow rate. (Çengel 2003)

3 COMPUTATIONAL FLUID DYNAMICS

Computational fluid dynamics (CFD) is a field of fluid mechanics that uses numerical methods and algorithms to solve and analyze fluid flows. Here the fluids are both liquids and gasses. The equations describing the flow of fluids are mainly partial differential equations (PDE) which combine the flow variables such as velocity, pressure, viscosity components etc. and their derivatives.

The main quantitative feature that is dealt with in CFD modeling is the *accuracy* of a numerical method, i.e., its ability to approximate the analytical solution of the given problem when the approximation tools become fine enough. The main qualitative feature taken into account is the *stability* of the method, i.e., its ability not to propagate and not to accumulate errors from the previous calculations into the following ones. The first step to numerically solve a given problem is its *numerical discretization.* This means that each component of the differential or PDE is transformed into a "numerical analogue" which can be represented on computer and then processed by a computer program, which is built on some algorithm. (Petrilia et al., 2005) The models of fluid flow are based on basic physical principles, such as the *conservation of mass, momentum, and energy* (Kuzmin 2010). A rapid change of several degrees in temperature may cause significant fluctuations in viscosity and further in the inner stresses of the fluid.

The use of a universally suitable model makes it rather difficult to develop and put into practice an efficient numerical algorithm. In many cases the demanded information can be obtained using a simplified version that exploits some priori knowledge of the flow pattern or contains empirical correlations supported by theoretical or experimental studies. (Kuzmin 2010) The basis of the fluid dynamics (fluids in motion) and CFD are the *Navier-Stokes equations.* They need to be resolved numerically (Equation 12).

$$\overbrace{\rho \underbrace{\frac{\partial \boldsymbol{v}}{\partial t}}_{\text{IV}} + \rho \underbrace{(\boldsymbol{v}\cdot\boldsymbol{\nabla})\boldsymbol{v}}_{\text{V}}}^{\text{I}} = \overbrace{\underbrace{\boldsymbol{\nabla}\cdot[-p\boldsymbol{I}]}_{\text{VI}} + \underbrace{\mu(\boldsymbol{\nabla}\boldsymbol{v} + (\boldsymbol{\nabla}\boldsymbol{v})^T) - \frac{2}{3}\mu(\boldsymbol{\nabla}\cdot\boldsymbol{v})\boldsymbol{I}]}_{\text{VII}}}^{\text{II}} + \overbrace{\boldsymbol{F}}^{\text{III}} \qquad (12)$$

Where: **I** is *Inertia* (per volume), **II** is *Divergence of stress*, **III** is *Other body forces* (e.g. gravity), **IV** is *Convective acceleration*, **V** is *Unsteady acceleration*, **VI** is *Pressure gradient*, **VII** is *Viscosity*, ρ is density, $\frac{\partial \boldsymbol{v}}{\partial \mathrm{t}}$ is time-dependent change in velocity (acceleration), $\boldsymbol{\nabla}$ is Nabla – operator, p is pressure, $\boldsymbol{I}$ is unit vector, μ is dynamic viscosity, and $\boldsymbol{F}$ is external force-vector. Equation 12 is common expression for *Navier-Stokes equations* and it does not tell which coordinate system is handled.

Below is shown *Navier-stokes equation* in cartesian, cylindrical, and spherical coordinate expression (Equations 13-21). Modeling heat collection pipes three-dimensionally requires cylindrical coordinate expression, and modeling fluid flow in free space requires spherical coordinate expression. (Kuzmin 2010, 2011; Petrilia et al., 2005; Wikipedia 2011: Computational Fluid Dynamics)

Navier-Stokes equations in cartesian coordinate expression

x-direction (13)

$$\rho\left(\frac{\partial \boldsymbol{v}_\mathrm{x}}{\partial t}+\boldsymbol{v}_\mathrm{x}\frac{\partial \boldsymbol{v}_\mathrm{x}}{\partial x}+\boldsymbol{v}_\mathrm{y}\frac{\partial \boldsymbol{v}_\mathrm{x}}{\partial y}+\boldsymbol{v}_\mathrm{z}\frac{\partial \boldsymbol{v}_\mathrm{x}}{\partial z}\right)=-\frac{\partial p}{\partial x}+\mu\left[\frac{\partial^2 \boldsymbol{v}_\mathrm{x}}{\partial x^2}+\frac{\partial^2 \boldsymbol{v}_\mathrm{x}}{\partial y^2}+\frac{\partial^2 \boldsymbol{v}_\mathrm{x}}{\partial z^2}\right]+\rho \boldsymbol{g}_\mathrm{x}$$

y-direction (14)

$$\rho\left(\frac{\partial \boldsymbol{v}_\mathrm{y}}{\partial t}+\boldsymbol{v}_\mathrm{x}\frac{\partial \boldsymbol{v}_\mathrm{y}}{\partial x}+\boldsymbol{v}_\mathrm{y}\frac{\partial \boldsymbol{v}_\mathrm{y}}{\partial y}+\boldsymbol{v}_\mathrm{z}\frac{\partial \boldsymbol{v}_\mathrm{y}}{\partial z}\right)=-\frac{\partial p}{\partial y}+\mu\left[\frac{\partial^2 \boldsymbol{v}_\mathrm{y}}{\partial x^2}+\frac{\partial^2 \boldsymbol{v}_\mathrm{y}}{\partial y^2}+\frac{\partial^2 \boldsymbol{v}_\mathrm{y}}{\partial z^2}\right]+\rho \boldsymbol{g}_\mathrm{y}$$

z-direction (15)

$$\rho\left(\frac{\partial \boldsymbol{v}_\mathrm{z}}{\partial t}+\boldsymbol{v}_\mathrm{x}\frac{\partial \boldsymbol{v}_\mathrm{z}}{\partial x}+\boldsymbol{v}_\mathrm{y}\frac{\partial \boldsymbol{v}_\mathrm{z}}{\partial y}+\boldsymbol{v}_\mathrm{z}\frac{\partial \boldsymbol{v}_z}{\partial z}\right)=-\frac{\partial p}{\partial z}+\mu\left[\frac{\partial^2 \boldsymbol{v}_\mathrm{z}}{\partial x^2}+\frac{\partial^2 \boldsymbol{v}_\mathrm{z}}{\partial y^2}+\frac{\partial^2 \boldsymbol{v}_\mathrm{z}}{\partial z^2}\right]+\rho \boldsymbol{g}_\mathrm{z}$$

Where: $\boldsymbol{v}_{\mathrm{x}}$ is velocity vector - on the direction of x, $\boldsymbol{v}_{\mathrm{y}}$ is velocity vector - on the direction of y, $\boldsymbol{v}_{\mathrm{z}}$ is velocity vector - on the direction of z, $\boldsymbol{g}_{\mathrm{x}}$ is gravity constant vector - on the direction of x, $\boldsymbol{g}_{\mathrm{y}}$ is gravity constant vector - on the direction of y and $\boldsymbol{g}_{\mathrm{z}}$ is gravity constant vector - on the direction of z. x, y and z are the coordinate axels in the cartesian coordinate system.

Navier-Stokes equations in cylindrical coordinate expression

r-direction (16)

$$\rho\left(\frac{\partial \boldsymbol{v}_{\mathrm{r}}}{\partial t}+\boldsymbol{v}_{\mathrm{r}}\frac{\partial \boldsymbol{v}_{\mathrm{r}}}{\partial r}+\frac{\boldsymbol{v}_{\phi}}{r}\frac{\partial \boldsymbol{v}_{\mathrm{r}}}{\partial \phi}+\boldsymbol{v}_{\mathrm{z}}\frac{\partial \boldsymbol{v}_{\mathrm{r}}}{\partial z}-\frac{{\boldsymbol{v}_{\phi}}^{2}}{r}\right) = -\frac{\partial p}{\partial r}+\mu\left[\frac{1}{r}\frac{\partial}{\partial r}\left(r\frac{\partial \boldsymbol{v}_{\mathrm{r}}}{\partial r}\right)+\frac{1}{r^{2}}\frac{\partial^{2}\boldsymbol{v}_{\mathrm{r}}}{\partial \phi^{2}}+\frac{\partial^{2}\boldsymbol{v}_{\mathrm{r}}}{\partial z^{2}}-\frac{\boldsymbol{v}_{\mathrm{r}}}{r^{2}}-\frac{2}{r^{2}}\frac{\partial \boldsymbol{v}_{\phi}}{\partial \phi}\right]+\rho\boldsymbol{g}_{\mathrm{r}}$$

ϕ-direction (17)

$$\rho\left(\frac{\partial \boldsymbol{v}_{\phi}}{\partial t}+\boldsymbol{v}_{\mathrm{r}}\frac{\partial \boldsymbol{v}_{\phi}}{\partial r}+\frac{\boldsymbol{v}_{\phi}}{r}\frac{\partial \boldsymbol{v}_{\phi}}{\partial \phi}+\boldsymbol{v}_{\mathrm{z}}\frac{\partial \boldsymbol{v}_{\phi}}{\partial z}+\frac{\boldsymbol{v}_{\mathrm{r}}\boldsymbol{v}_{\phi}}{r}\right) = -\frac{1}{r}\frac{\partial p}{\partial \phi}+\mu\left[\frac{1}{r}\frac{\partial}{\partial r}\left(r\frac{\partial \boldsymbol{v}_{\phi}}{\partial r}\right)+\frac{1}{r^{2}}\frac{\partial^{2}\boldsymbol{v}_{\phi}}{\partial \phi^{2}}+\frac{\partial^{2}\boldsymbol{v}_{\phi}}{\partial z^{2}}+\frac{2}{r^{2}}\frac{\partial \boldsymbol{v}_{r}}{\partial \phi}-\frac{\boldsymbol{v}_{\phi}}{r^{2}}\right]+\rho\boldsymbol{g}_{\phi}$$

z-direction (18)

$$\rho\left(\frac{\partial \boldsymbol{v}_{\mathrm{z}}}{\partial t}+\boldsymbol{v}_{\mathrm{r}}\frac{\partial \boldsymbol{v}_{\mathrm{z}}}{\partial r}+\frac{\boldsymbol{v}_{\phi}}{r}\frac{\partial \boldsymbol{v}_{\mathrm{z}}}{\partial \phi}+\boldsymbol{v}_{\mathrm{z}}\frac{\partial \boldsymbol{v}_{\mathrm{z}}}{\partial z}\right) = -\frac{\partial p}{\partial r}+\mu\left[\frac{1}{r}\frac{\partial}{\partial r}\left(r\frac{\partial \boldsymbol{v}_{\mathrm{z}}}{\partial r}\right)+\frac{1}{r^{2}}\frac{\partial^{2}\boldsymbol{v}_{\mathrm{z}}}{\partial \phi^{2}}+\frac{\partial^{2}\boldsymbol{v}_{\mathrm{z}}}{\partial z^{2}}\right]+\rho\boldsymbol{g}_{\mathrm{z}}$$

Where: $\boldsymbol{v}_{\mathrm{r}}$ is velocity vector - on the direction of r, $\boldsymbol{v}_{\phi}$ is velocity vector - on the direction of ϕ, $\boldsymbol{g}_{\mathrm{r}}$ is gravity constant vector - on the direction of r, $\boldsymbol{g}_{\phi}$ is gravity constant vector - on the direction of ϕ. r, ϕ and z are the coordinate axels in the cylindrical coordinate system.

Navier-Stokes equations in spherical coordinate expression

r-direction (19)

$$\rho\left(\frac{\partial \boldsymbol{v}_\mathrm{r}}{\partial t}+\boldsymbol{v}_\mathrm{r}\frac{\partial \boldsymbol{v}_\mathrm{r}}{\partial r}+\frac{\boldsymbol{v}_\phi}{r\sin(\theta)}\frac{\partial \boldsymbol{v}_\mathrm{r}}{\partial \phi}+\frac{\boldsymbol{v}_\theta}{r}\frac{\partial \boldsymbol{v}_\mathrm{r}}{\partial \theta}-\frac{{\boldsymbol{v}_\phi}^2+{\boldsymbol{v}_\theta}^2}{r}\right)$$
$$=-\frac{\partial p}{\partial r}+\mu\left[\frac{1}{r^2}\frac{\partial}{\partial r}\left(r^2\frac{\partial \boldsymbol{v}_\mathrm{r}}{\partial r}\right)+\frac{\boldsymbol{v}_\phi}{r^2\sin(\theta)^2}\frac{\partial^2 \boldsymbol{v}_\mathrm{r}}{\partial \phi^2}+\frac{1}{r^2\sin(\theta)}\frac{\partial}{\partial \theta}\left(\sin(\theta)\frac{\partial \boldsymbol{v}_\mathrm{r}}{\partial \theta}\right)-2\frac{\boldsymbol{v}_\mathrm{r}+\frac{\partial \boldsymbol{v}_\theta}{\partial \theta}+\boldsymbol{v}_\theta\cot(\theta)}{r^2}-\frac{2}{r^2\sin(\theta)}\frac{\partial \boldsymbol{v}_\theta}{\partial \theta}\right]+\rho\boldsymbol{g}_\mathrm{r}$$

ϕ-direction (20)

$$\rho\left(\frac{\partial \boldsymbol{v}_\phi}{\partial t}+\boldsymbol{v}_\mathrm{r}\frac{\partial \boldsymbol{v}_\phi}{\partial r}+\frac{\boldsymbol{v}_\phi}{r\sin(\theta)}\frac{\partial \boldsymbol{v}_\phi}{\partial \phi}+\frac{\boldsymbol{v}_\theta}{r}\frac{\partial \boldsymbol{v}_\phi}{\partial \theta}+\frac{\boldsymbol{v}_\mathrm{r}\boldsymbol{v}_\phi+\boldsymbol{v}_\phi\boldsymbol{v}_\theta\cot(\theta)}{r}\right)$$
$$=-\frac{1}{r\sin(\theta)}\frac{\partial p}{\partial \phi}+\mu\left[\frac{1}{r^2}\frac{\partial}{\partial r}\left(r^2\frac{\partial \boldsymbol{v}_\phi}{\partial r}\right)+\frac{1}{r^2\sin(\theta)^2}\frac{\partial^2 \boldsymbol{v}_\phi}{\partial \phi^2}+\frac{1}{r^2\sin(\theta)}\frac{\partial}{\partial \theta}\left(\sin(\theta)\frac{\partial \boldsymbol{v}_\phi}{\partial \theta}\right)+\frac{2\sin(\theta)\frac{\partial \boldsymbol{v}_\mathrm{r}}{\partial \theta}+2\cos(\theta)\frac{\partial \boldsymbol{v}_\theta}{\partial \phi}-\boldsymbol{v}_\phi}{r^2\sin(\theta)^2}\right]$$
$$+\rho\boldsymbol{g}_\phi$$

θ-direction (21)

$$\rho\left(\frac{\partial \boldsymbol{v}_\theta}{\partial t}+\boldsymbol{v}_\mathrm{r}\frac{\partial \boldsymbol{v}_\theta}{\partial r}+\frac{\boldsymbol{v}_\theta}{r\sin(\theta)}\frac{\partial \boldsymbol{v}_\theta}{\partial \phi}+\frac{\boldsymbol{v}_\theta}{r}\frac{\partial \boldsymbol{v}_\theta}{\partial \theta}+\frac{\boldsymbol{v}_\mathrm{r}\boldsymbol{v}_\theta-{\boldsymbol{v}_\phi}^2\cot(\theta)}{r}\right)$$
$$=-\frac{1}{r}\frac{\partial p}{\partial \theta}+\mu\left[\frac{1}{r^2}\frac{\partial}{\partial r}\left(r^2\frac{\partial \boldsymbol{v}_\theta}{\partial r}\right)+\frac{1}{r^2\sin(\theta)^2}\frac{\partial^2 \boldsymbol{v}_\theta}{\partial \phi^2}+\frac{1}{r^2\sin(\theta)}\frac{\partial}{\partial \theta}\left(\sin(\theta)\frac{\partial \boldsymbol{v}_\theta}{\partial \theta}\right)+\frac{2}{r^2}\frac{\partial \boldsymbol{v}_\mathrm{r}}{\partial \theta}-\frac{\boldsymbol{v}_\theta+2\cos(\theta)\frac{\partial \boldsymbol{v}_\phi}{\partial \phi}}{r^2\sin(\theta)^2}\right]+\rho\boldsymbol{g}_\theta$$

Where: $\boldsymbol{v}_\theta$ is velocity vector - on the direction of θ. $\boldsymbol{g}_\theta$ is gravity constant vector - on the direction of θ. r, ϕ and θ are the coordinate axels in the spherical coordinate system. *Navier-Stokes equations* can be simplified by removing the terms describing viscosity and vorticity (Wikipedia 2011: Computational Fluid Dynamics).

CFD analysis process is based on the following steps (Kuzmin 2010, 2011):

A. DEFINING THE FLOW PROBLEM

1. Problem statement → information about the flow

Following issues need to be solved:

- what is known about the flow problem to be dealt with
- what physical phenomena need to be taken into account
- what is the geometry of the domain and operating conditions
- are there any internal obstacles or free surfaces/interfaces
- what is the type of flow (laminar/transitional/turbulent, steady/unsteady)
- what is the objective of the CFD analysis to be performed
- computation of integral quantities (lift, drag, yield)
- snapshots of field data for velocities, concentrations etc.
- shape optimization aimed at an improved performance
- what is the easiest/cheapest/fastest way to achieve the goal

B. BUILDING THE MATHEMATICAL MODEL

2. Mathematical model → IBVP = PDE + IC + BC

where: IBVP is initial boundary value problem, PDE is partial differential equation, IC is initial conditions and BC is boundary conditions.

Following issues need to be solved:

- choosing a suitable flow model (viewpoint) and reference frame
- identifying the forces which cause and influence the fluid motion
- defining the computational domain in which to solve the problem
- formulating conservation laws for the mass, momentum, and energy
- simplifying the governing equations to reduce the computational effort:
    - using available information about the prevailing flow regime
    - checking for symmetries and predominant flow directions (1D/2D)
    - neglecting the terms which have little or no influence on the results
    - modeling the effect of small-scale fluctuations that cannot be captured
    - incorporating a priori knowledge (measurement data, CFD results)
    - adding constitutive relations and specify initial/boundary conditions

C. DISCRETIZATION

3. Mesh generation → node/cells, time instant
4. Space discretization → coupled ODE/DAE systems

where: ODE is ordinary differential equation and DAE is differential algebraic equation

5. Time discretization → algebraic systems → $Ax=b$

Following issues need to be solved for the discretization:

- the PDE system is transformed into a set of algebraic equations
- mesh generation (decomposition into cells/elements)
  - structured or unstructured, triangular or quadrilateral
  - CAD tools + grid generators (Delaunay, advancing front)
  - mesh size, adaptive refinement in "interesting" flow regions
- space discretization (approximation of spatial derivatives)
  - finite differences/volumes/elements
  - high- vs. low-order approximations
- time discretization (approximation of temporal derivatives)
  - explicit vs. implicit schemes, stability constraints
  - local time-stepping, adaptive time step control

D. ITERATION

6. Iterative solver → discrete function values

Following issues need to be solved:

- the coupled nonlinear algebraic equations must be solved iteratively
  - *outer iterations*: the coefficients of the discrete problem are updated using the solution values from the previous iteration so as to:
    - get rid of the nonlinearities by a Newton-like method
    - solve the governing equations in a segregated fashion
  - *inner iterations*: the resulting sequence of linear sub-problems is typically solved by an iterative method (conjugate gradients, multigrid) because direct solvers (Gaussian elimination) are prohibitively expensive
  - *convergence criteria*: it is necessary to check the residuals, relative solution changes and other indicators to make sure that the iterations converge

E. SIMULATION PROCESS

7. CFD software	→	implementation, debugging
8. Simulation run	→	parameters, stopping criteria
9. Postprocessing	→	visualization, analysis of data
10. Verification	→	model validation/adjustment

The above mentioned issues can be divided into following steps:

1. Consistency:
   - the discretization of a PDE should become exact as the mesh size tends to zero → truncation error should vanish
2. Stability:
   - numerical errors which are generated during the solution of discretized equations should not be magnified
3. Convergence:
   - the numerical solution should approach the exact solution of the PDE and converge to it as the mesh size tends to zero
4. Conservation:
   - underlying conservation laws should be respected at the discrete level → artificial sources/sinks are to be avoided
5. Boundedness:
   - densities, temperatures, concentrations etc. quantities should remain nonnegative and free of spurious wiggles

Every step is crucially important in the whole CFD model process, but discretization is the most influential step. It is based on mathematical equations and the model accuracy is dependent on its role. These lead us to the basis of CFD modeling: *numerical algorithms,* which are crucial to the performance of the whole CFD modeling process. Macroscopic properties in fluid characteristics are: density, dynamic viscosity, pressure, temperature and velocity. The classification of fluid flows can be obtained from these and they are: viscous → inviscous, compressible → incompressible, steady → unsteady, laminar → turbulent, single-phase → multiphase. (Kuzmin 2011)

4 DIFFERENT MODELING METHODS

There are several different methods which can be used to solve problems related to fluid flow behavior, e.g. finite difference method (FDM), finite volume method (FVM), and finite element method (FEM). When modeling turbulent fluid flow behavior, commonly used equations are *Reynolds Average Navier-Stokes equations* (RANS) (Equation 22) and there the *k-ε* flow model is used. (COMSOL Multiphysics 2011)

$$\rho\frac{\partial \boldsymbol{V}}{\partial \mathrm{t}} + \rho(\boldsymbol{V}\cdot\boldsymbol{\nabla})\boldsymbol{V} + \boldsymbol{\nabla}\cdot\overline{(\rho\boldsymbol{v}'\otimes\boldsymbol{v}')} = \boldsymbol{\nabla}\cdot\left[-p\boldsymbol{I} + \mu(\boldsymbol{\nabla V} + (\boldsymbol{\nabla V})^{T}) - \frac{2}{3}\mu(\boldsymbol{\nabla}\cdot\boldsymbol{V})\boldsymbol{I}\right] + \boldsymbol{F} \qquad (22)$$

$$\frac{\partial \rho}{\partial \mathrm{t}} + \boldsymbol{\nabla}\cdot(\rho\boldsymbol{V}) = 0$$

Where: $\otimes$ is outer vector product and $\boldsymbol{V}$ is averaged velocity vector. The only difference between Equations 12 and 22 is the last term of the left-hand side of Equation 22 (the yellow one). That term represents interaction between the fluctuating velocities and it is the *Reynolds stress tensor*. This means that to obtain the mean flow characteristics, the information about the minor-scale structure of the flow has to be available. In this case that information is the correlation between fluctuations in different directions (COMSOL Multiphysics 2011: *RANS*). Turbulence fluid flow could be calculated in a purely analytical way if there were computing capacity enough. At this point it needs to be calculated and modeled by averaging. One way is to calculate large eddies and model small eddies.

4.1 The Finite Difference Method

The principle of the finite difference method (FDM) is: derivatives in the PDE are approximated by linear combinations of function values at the grid points. The *Taylor series* is used instead of integral equations. FDM is the oldest discretization technique for PDEs and it was developed between the late 1950's and early 1980's. The derivation and implementation of FDM is especially simple with structured meshes, which are topologically corresponding to the coherent cartesian grid.

FDM's solution's error is defined as the difference between its approximation and the exact analytical solution. The first step when using FDM to approximate the solution is to discretize the domain of the problem. In general, this means that the domain of the problem is divided into uniform grids. Therefore, FDM produces sets of discrete numerical approximations to the derivative in a time-stepping manner. So the basic idea of FDM is to replace the derivatives appearing in the PDEs or ordinary differential equations (ODE) by finite differences that approximate them. FDM is basically based on one-dimensional approximating techniques. (Kuzmin 2010, 2011; Wikipedia 2011: Finite Difference Method)

4.2 The Finite Volume Method

The Finite volume method (FVM) replaced FDM when demand for two-dimensional and three-dimensional CFD modeling grew. Nowadays most of the CFD codes are based on FVM, which yields much more suitable solutions for unstructured meshes than FDM. FVM is based on PDEs and integral conservation laws, which are based on the usage of control volumes. FVM represents and evaluates PDEs in the form of algebraic equations. In FVM, values of discrete places are calculated using meshed geometry. So in FVM, PDEs are converted into surface integrals by using the *divergence theorem*. The theory of fluid dynamics or CFD is mainly based on finite volumes to represent the geometry in the domains of the problem. This means that the domain of the problem is divided into boxes with finite volumes. (Kuzmin 2010, 2011; Wikipedia 2011: Finite Volume Method)

4.3 The Finite Element Analysis and the Finite Element Method

In this thesis the method used is the finite element method (FEM), and the modeling software is COMSOL Multiphysics. FEM must be carefully formulated and the formulation requires special care to ensure a conservative solution. FEM is somewhat newer technique than FDM or FVM. FEM is a very suitable technique both in mechanical and thermal stresses in CFD problems (FEM was designed first to model structural mechanics (Figure 7), but quite fast it was noticed that it can be modified into the use of model CFD problems as well). FEM provides the best approximation properties when applied to elliptic and parabolic problems. The mathematical theory behind the FEM enables the obtaining of exact error estimates and proofs of convergence. (Kuzmin 2010, 2011)

Finite element analysis (FEA) and FEM are methods for finding solutions for PDE as well as for integral equations. The most challenging issue when solving PDEs is to create an equation which approximates the equation but is at the same time numerically stable. This means that errors in the input and intermediate calculations do not accumulate and therefore make the results meaningless for the output. (Wikipedia 2011: Finite Element Method)

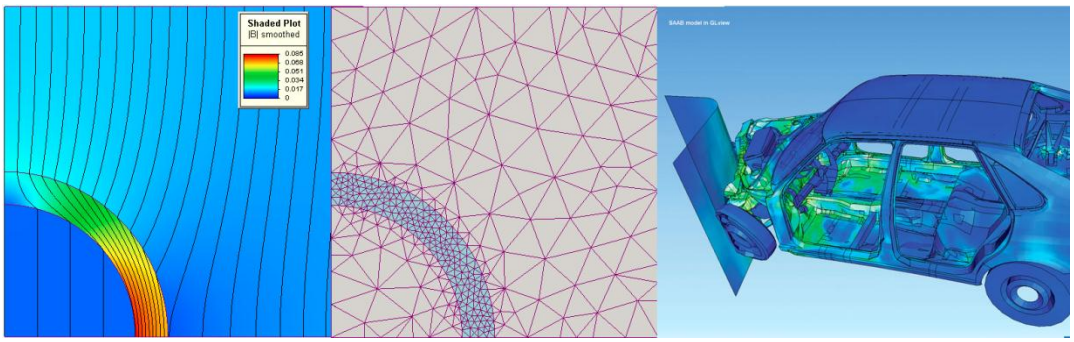

Figure 7. Figure 7. FEM Solutions for 2D- Magnetostatic Configuration (Left) and Meshing (Middle) and Visualization of how a Car Deforms in an Asymmetrical Crash (Right) (Wikipedia 2011: Finite Element Method)

The greatest advantage of FEM is that it is suitable for modeling complicated counting areas. Therefore there is no need to simplify the geometry for oblique or curved edges. FDM approximates the values of unknown functions pointwise at each nodes of the calculation lattice. In FEM, the values of unknown functions can be approximated inside of each element with linear or quadratic polynomial. Thus FEM is more suitable to use when modeling big physical systems which may contain CFD problems as well as structural stress problems (e.g. stresses inside pipe curves). In FVM the problem domain is divided into boxes with finite volume. In FEM the problem domain is divided into elements with finite area which produces element mesh for the whole domain (Figure 8). (Hämäläinen, Järvinen 2006)

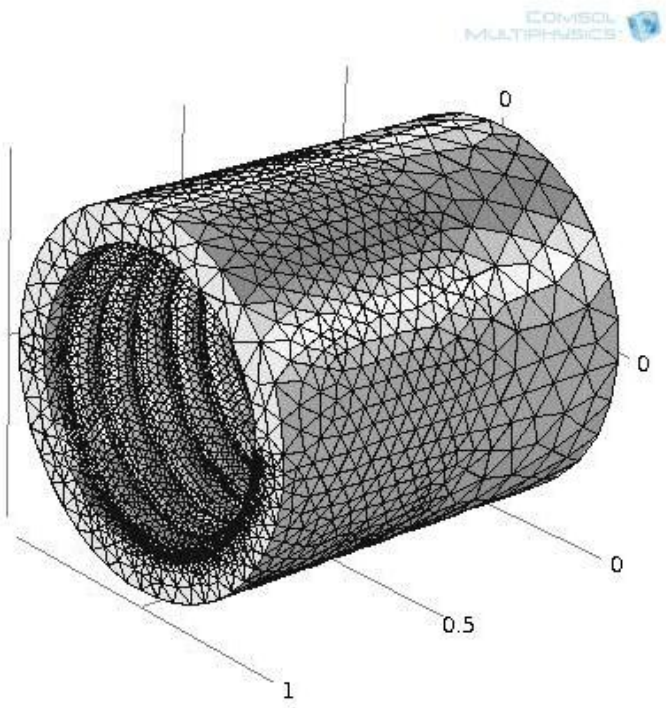

Figure 8. 3D-Mesh for Axially Placed Fins inside the Pipe

5 FLUID FLOW MODELING WITH COMSOL MULTIPHYSICS

Here was modeled fluid flow with the COMSOL Multiphysics software and its CFD module. COMSOL is FEM-based simulation & modeling software. Here was examined which kind of shape on the inner surface of the heat collection pipe has the most greatest effect on the flow behavior and what kind of shape is the best option to make the fluid flow more turbulent. As mentioned earlier, the flow behavior of heat collection fluid may change significantly if the temperature decreases, say for example three degrees. However, the high temperature of the heat collection fluid (or high flow velocity) does not alone guarantee fully developed turbulent flow. The fluid used in every model is pure ethanol.

Here was also examined how the flow behavior of the fluid changes if the inner surface structure of the heat collection pipe changes from smooth to somewhat finned. Smooth and finned inner profile is shown in Figure 9 in three-dimension. Here was also examined how a twisted tape inside the heat collection pipe changes the flow behavior. Pressure drop and pumping power requirements were also taken into account in every different pipe profile.

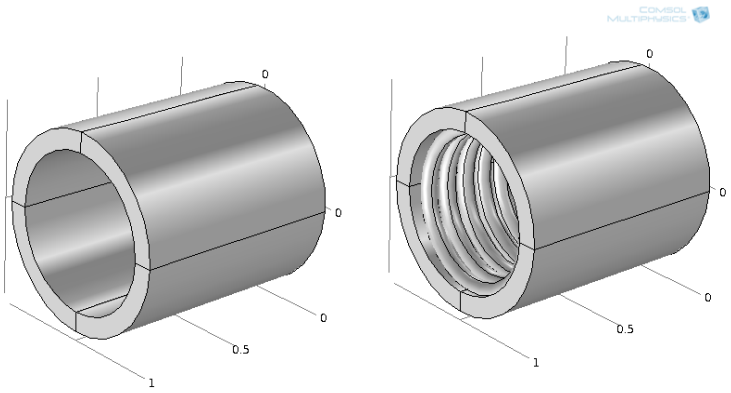

Figure 9. Smooth and Axial-Finned inside Profile

5.1 Smooth U-Pipe in 2D (Short)

Here was modeled how the flow behaves in a smooth-short u-pipe, before and after the u-turn. Here the time-dependent solver and a u-pipe profile were used (Figures 10 and 11). Inlet velocity is expressed with the step-function (Function 1) and the *flow equation* is expressed with Equation 23. Function 1 works as a pulse generator. In Equation 23 are the first-order time-dependent partial derivative from the velocity vector and the density (squared ones). On Figures 10 and 11 are shown the velocity- and pressure profiles when the fluid has flown 7 seconds. The length of the pipe was 5 m, the diameter was 40 mm and inlet flow velocity 1 m/s. Figure 14 shows how the velocity profile varies in the case of smooth-short u-pipe.

$$U\_mean * 6 * s * (1 - s) * \text{step1}(t[1/s]) \tag{1}$$

$$\boxed{\rho \frac{\partial \boldsymbol{v}}{\partial \mathrm{t}}} + \rho(\boldsymbol{v} \cdot \boldsymbol{\nabla})\boldsymbol{v} = \boldsymbol{\nabla} \cdot \left[-p\boldsymbol{I} + \mu(\boldsymbol{\nabla v} + (\boldsymbol{\nabla v})^T) - \frac{2}{3}\mu(\boldsymbol{\nabla} \cdot \boldsymbol{v})\boldsymbol{I}\right] + \boldsymbol{F} \tag{23}$$

$$\boxed{\frac{\partial \rho}{\partial \mathrm{t}}} + \boldsymbol{\nabla} \cdot (\rho \boldsymbol{v}) = 0$$

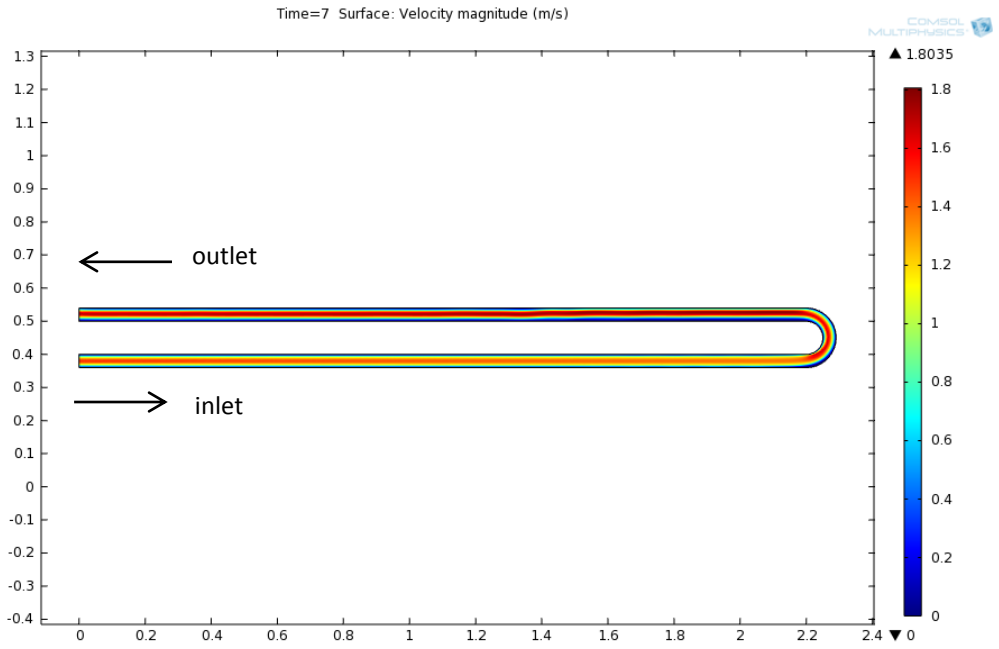

Figure 10. The Velocity Profile of a Smooth-Short U-Pipe

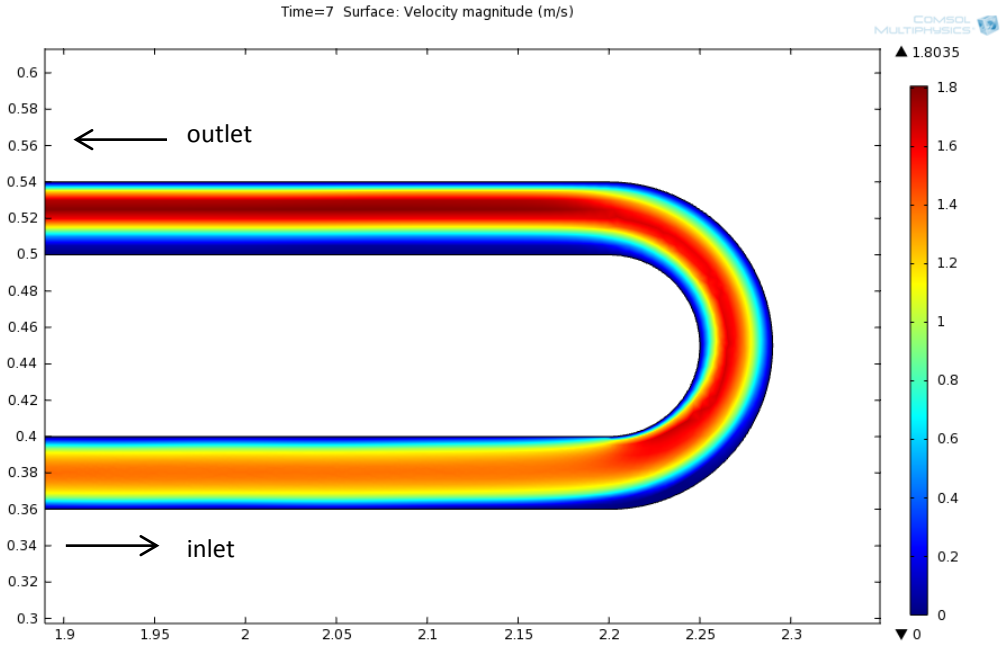

Figure 11. The Velocity Profile of a Smooth-Short U-Pipe (Zoomed)

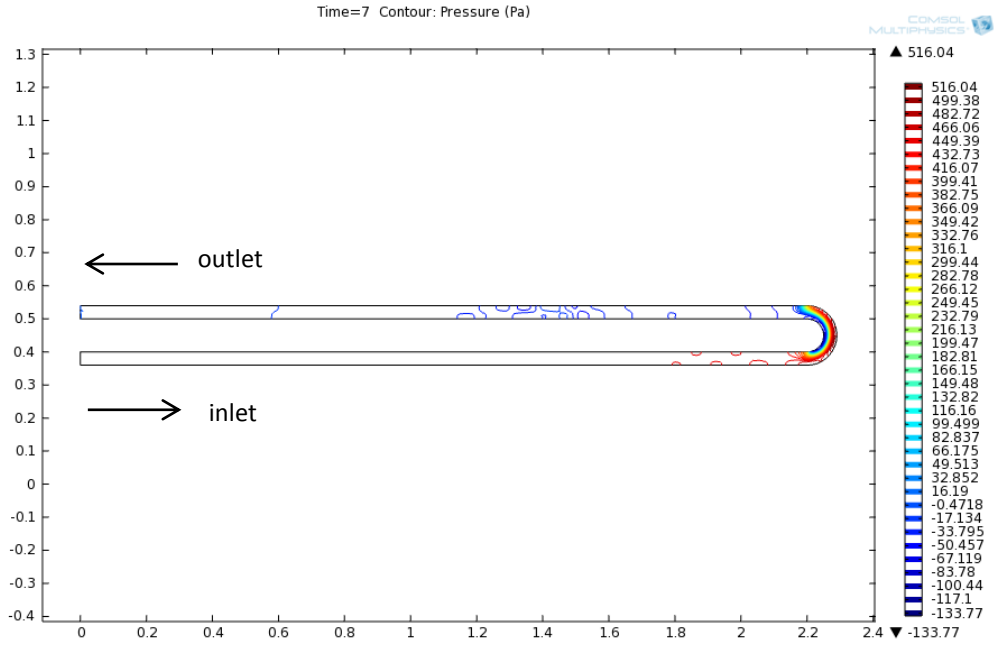

Figure 12. The Pressure Profile of a Smooth-Short U-Pipe

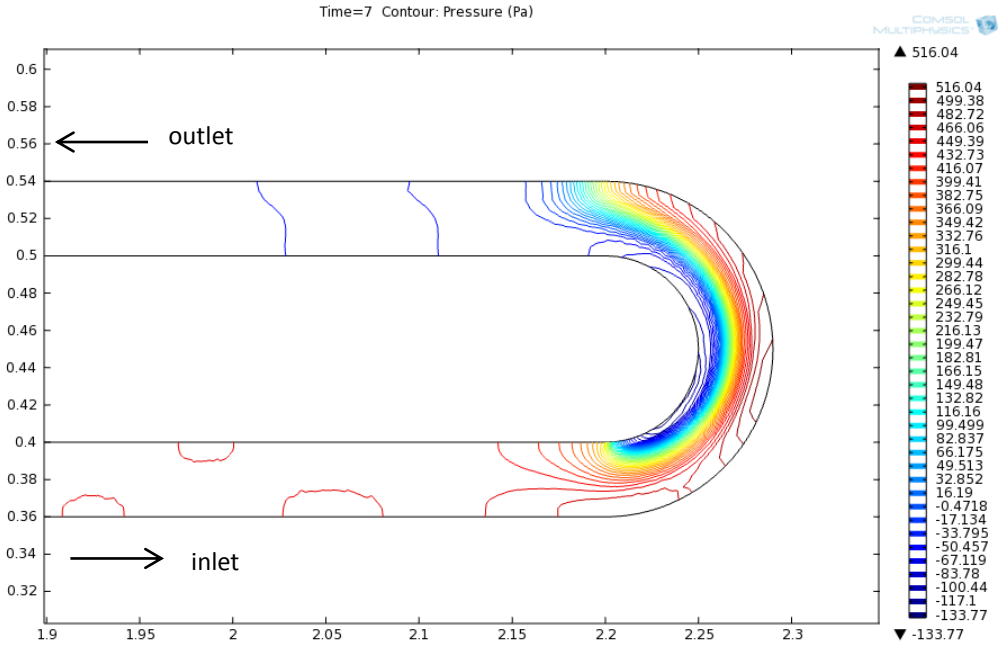

Figure 13. The Pressure Profile of a Smooth-Short U-Pipe (Zoomed)

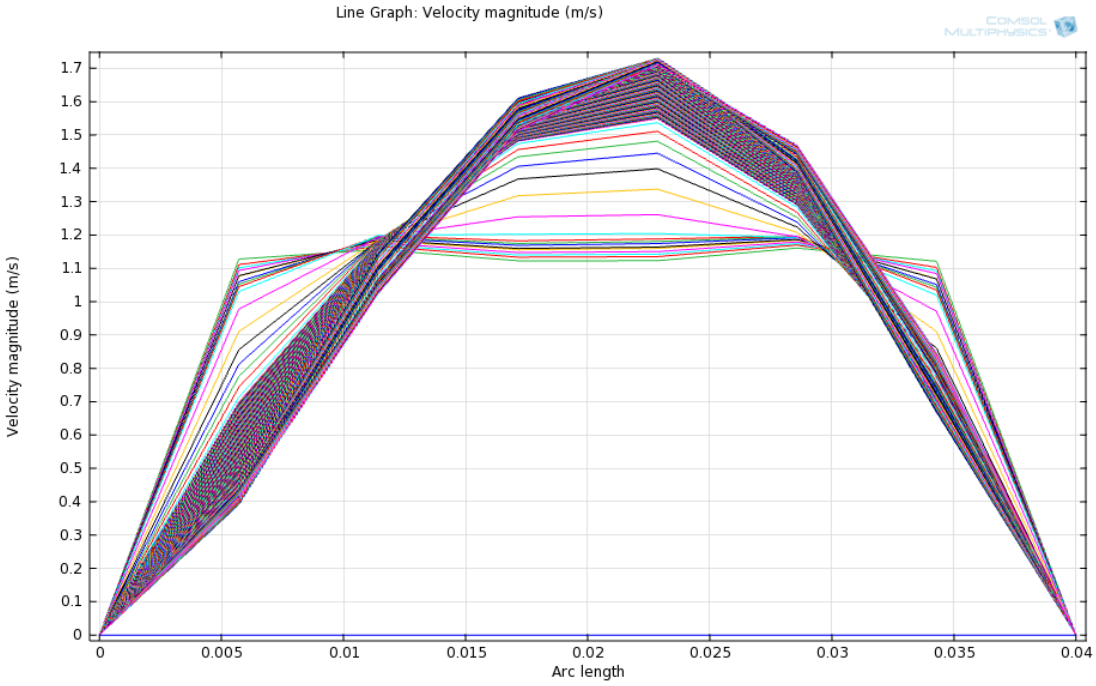

Figure 14. Velocity Profile Variations in a Smooth-Short U-Pipe

From Figures 10 and 11 it can be noticed that after the u-turn the velocity profile changes slightly in turbulence and also the pressure profile has fluctuations after the u-turn. Inside the smooth pipe both profiles stay quite stationary (laminar flow conditions) before the u-turn and here the heat transfer effect is not so great. Before the u-turn the velocity profile varies between 0.6 and 1.2 m/s and after the u-turn, velocity profile varies between 0.6 to 1.8 m/s. This yields velocity fluctuations and due to this slightly more turbulent flow behavior after the u-turn. The pressure differences occur actually only after the u-turn and their values vary approximately between -134 and 516 Pa. As a result, in case of smooth-short u-pipe, turbulence flow behavior can be achieved only after the u-turn. From Figure 14 it can be seen that the velocity profile follows to some extent a parabolic shape (Appendix 4). *Re* is between 2 630-47 340, but it is above 10 000 only for a while, so the flow behaved most of the time in transitional regime. Even though the *Re* has rather good ratios, the *eddying* motion is minor (Figures 10 and 11). So, in case of smooth-short u-pipe, the turbulent flow behavior is rather minor. The lines in Figure 14 represent different velocity areas in the flow.

5.2 Smooth U-Pipe in 2D (Long)

The geometry and setting values of this model (Figures 15 and 16) are the same as in the previous chapter. The only difference here is the length of the pipe, which was 100 meters. This is a suitable length in case of the heat collection pipes of a real GSHP system. Because of the longer pipe, the modeling process takes more time than when a short pipe is used. First it was planned to use a *cluster* – a calculation method to solve the meshing part and the computing phase. Unfortunately this was not carried out because the right kind of server was not available. The c*luster*-calculation method is based on a group of linked computers, working together via fast local network. Figures 15 and 16 are zoomed on the part of the heat collection pipe which is 26 meters from the inlet channel. Flow behavior was the same in every part of the pipe. Just before and after the u-turn, flow acted like is shown in Figure 10. In Figure 17 is shown how the velocity profile varies in case of the smooth pipe.

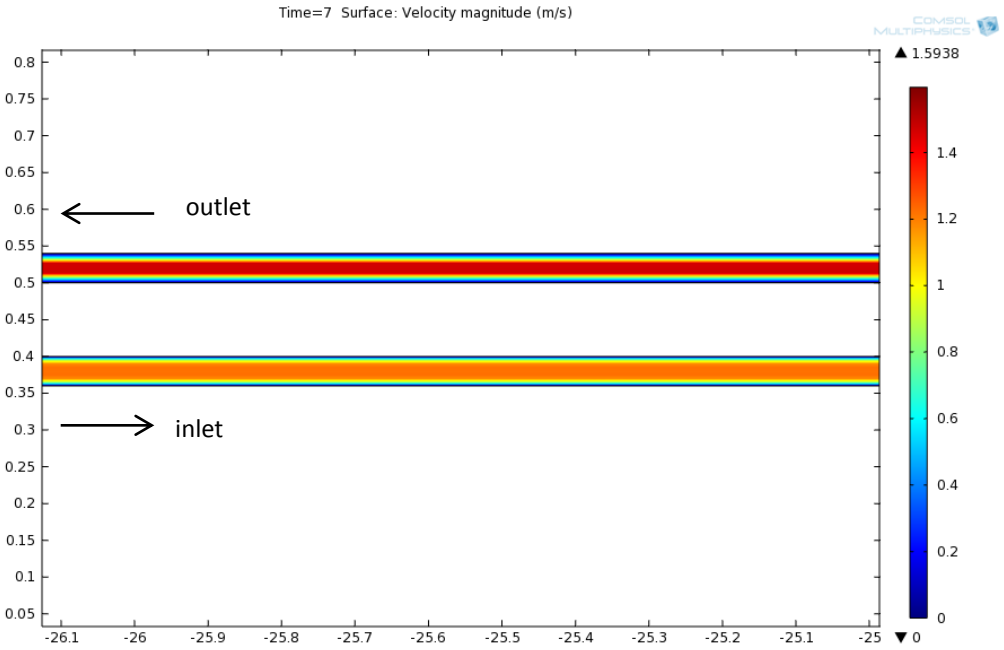

Figure 15. The Velocity Profile of a Smooth-Long U-Pipe

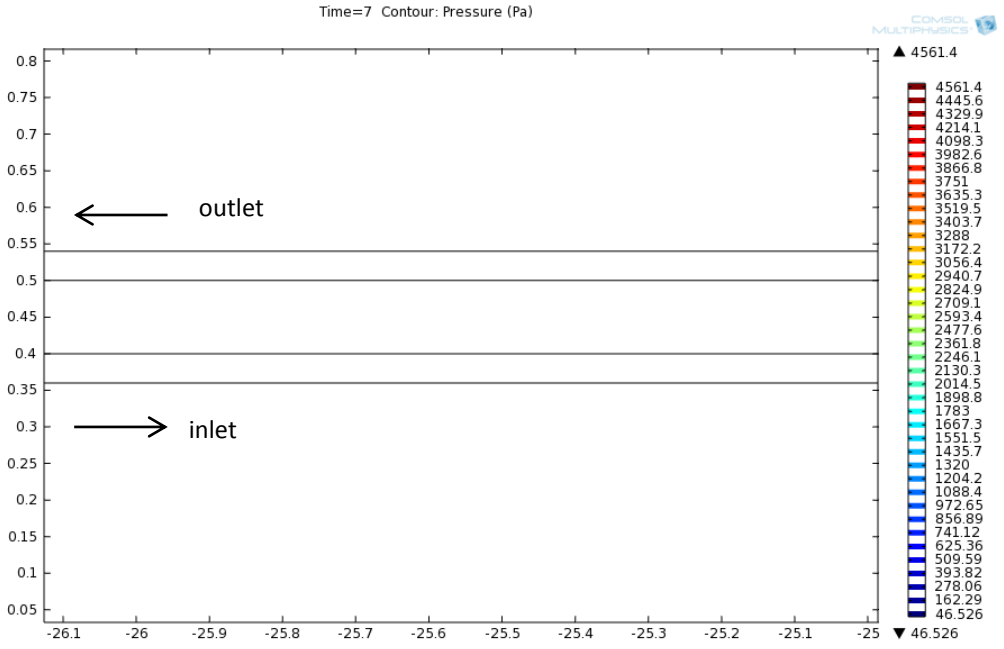

Figure 16. The Pressure Profile of a Smooth-Long U-Pipe

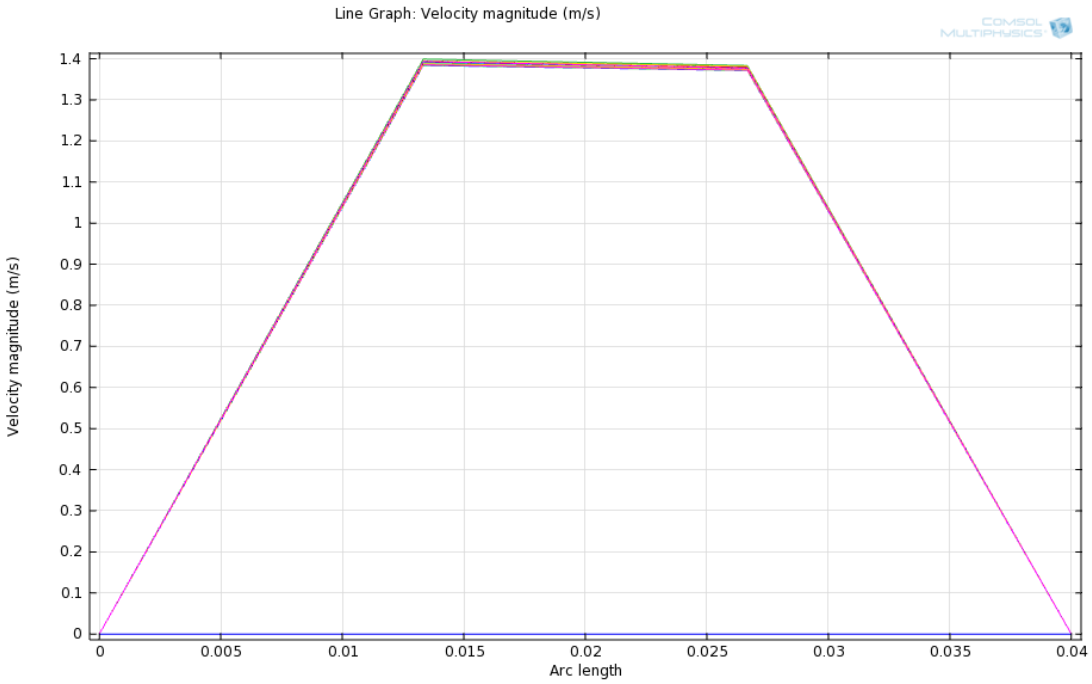

Figure 17. Velocity Profile Variations in a Smooth-Long U-Pipe

It can be noticed from Figure 15 that the velocity acted in a similar way as in Figure 10: it was laminar on the whole way before and after the u-turn. Before the u-turn the velocity profile varies between 0.6 and 1.2 m/s, after the u-turn it varies between 0.6 to 1.4 m/s. This yields velocity fluctuations and due to this slightly more turbulent flow behavior after the u-turn. The pressure differences occur actually only just after the u-turn and their values vary approximately between 46 Pa and 4.56 kPa. Because of this, in case of the smooth pipe, turbulence flow behavior can only be achieved just after the u-turn. In Figure 17 the *Re* is between 2 630-36 820, but it was above 10 000 only for a while. Although the *Re* had rather good ratios, the *eddying motion* is rather minor (Figures 10, 11 and 15). So the in case of the smooth pipe (both short and long) the turbulent flow behavior is rather minor. The lines in Figure 17 represent the different velocity areas in the flow.

5.3 Finned U-Pipe in 2D (Short)

Here was used the same geometry and setting values etc. as in the first example. Here a finned pipe profile instead of a straight pipe profile has been used (Figures 15 and 16). The inlet velocity is expressed here with the same step-function (Function 1) and the *flow equation* is expressed with Equation 23. Figures 18-21 show the velocity and pressure profiles when the fluid has flown for 7 seconds. The length of the pipe was 5 m, the diameter 40 mm and inlet flow velocity 1 m/s. This kind of a model takes slightly more time than a smooth pipe because of the modified inner surface structure, but every other setting is the same as in the previous model. In Figure 22 is shown how the velocity profile varies in case of a finned pipe.

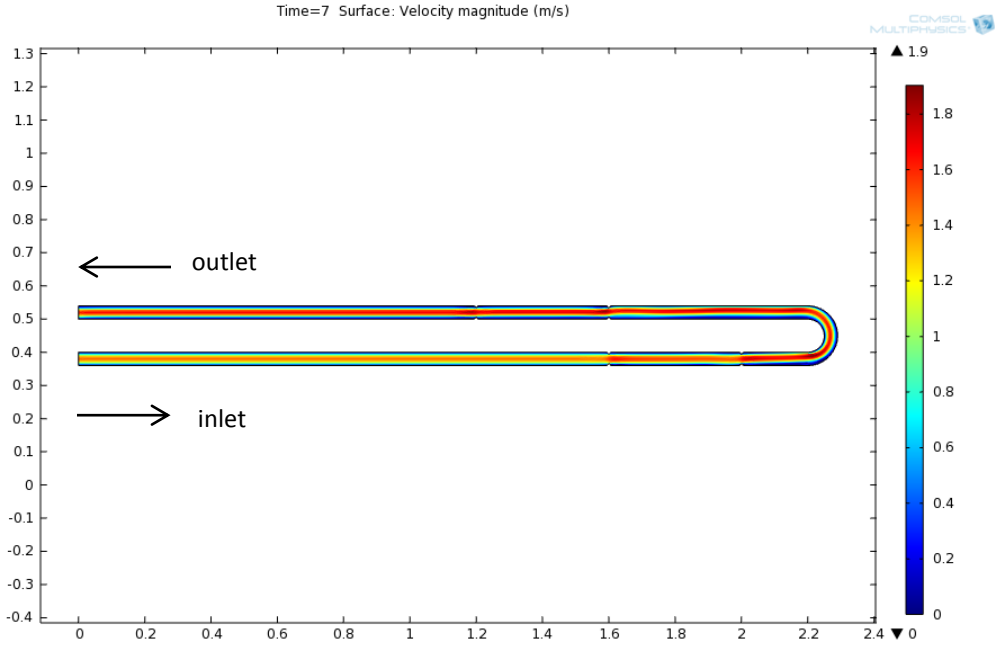

Figure 18. The Velocity Profile of a Finned-Short U-Pipe

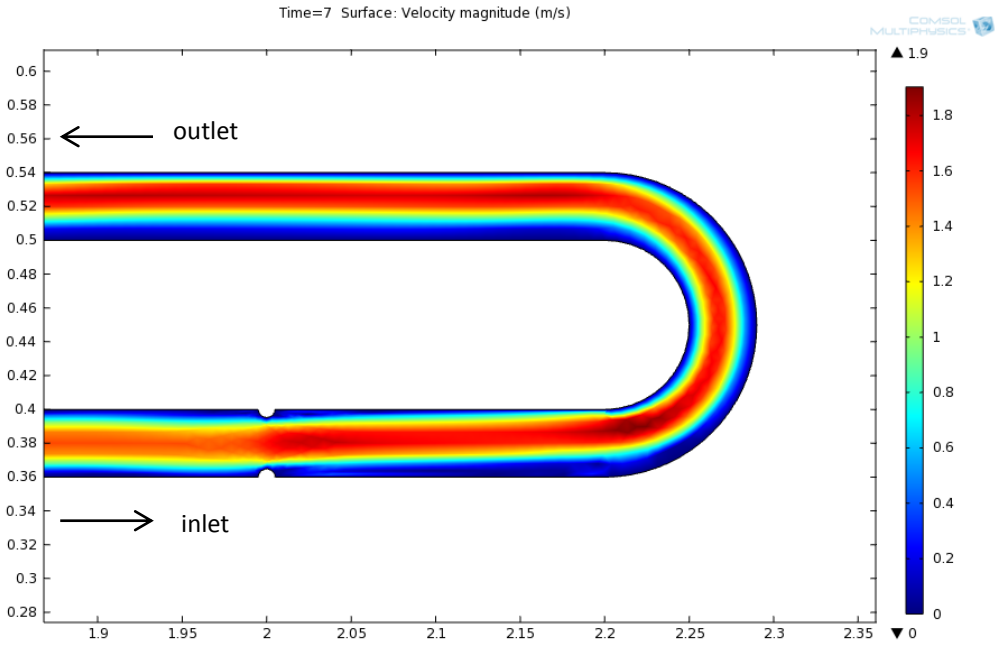

Figure 19. The Velocity Profile of the Finned-Short U-Pipe (Zoomed)

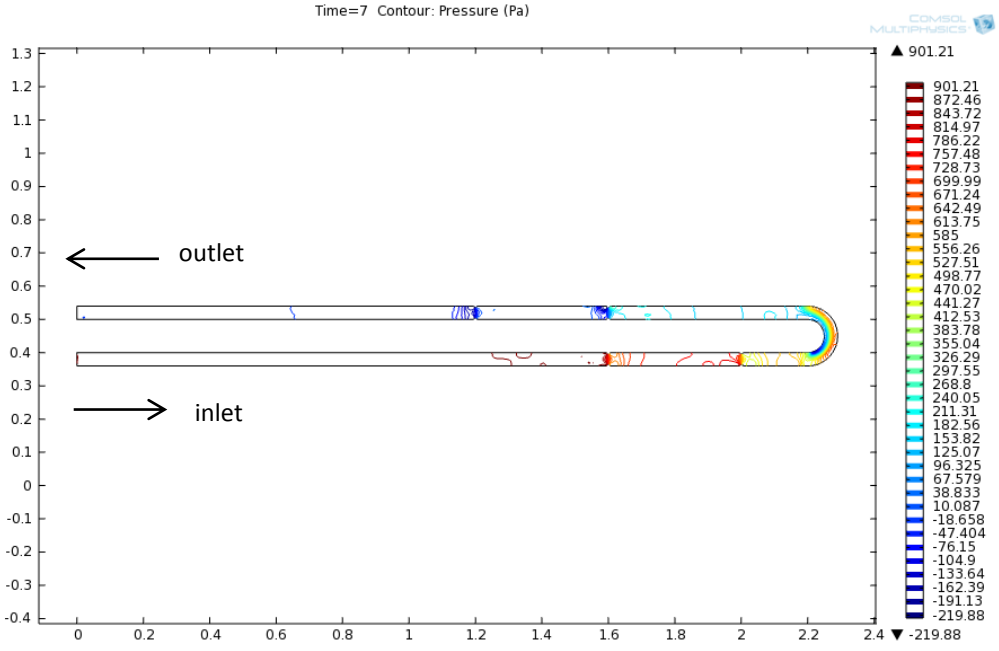

Figure 20. The Pressure Profile of a Finned-Short U-Pipe

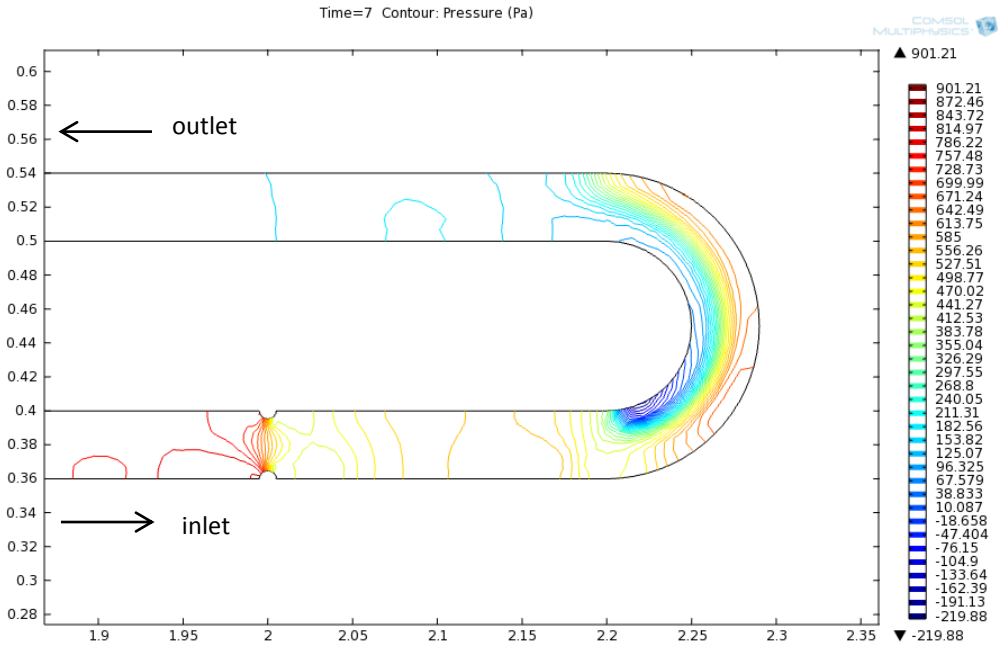

Figure 21. The Pressure Profile of a Finned-Short U-Pipe (Zoomed)

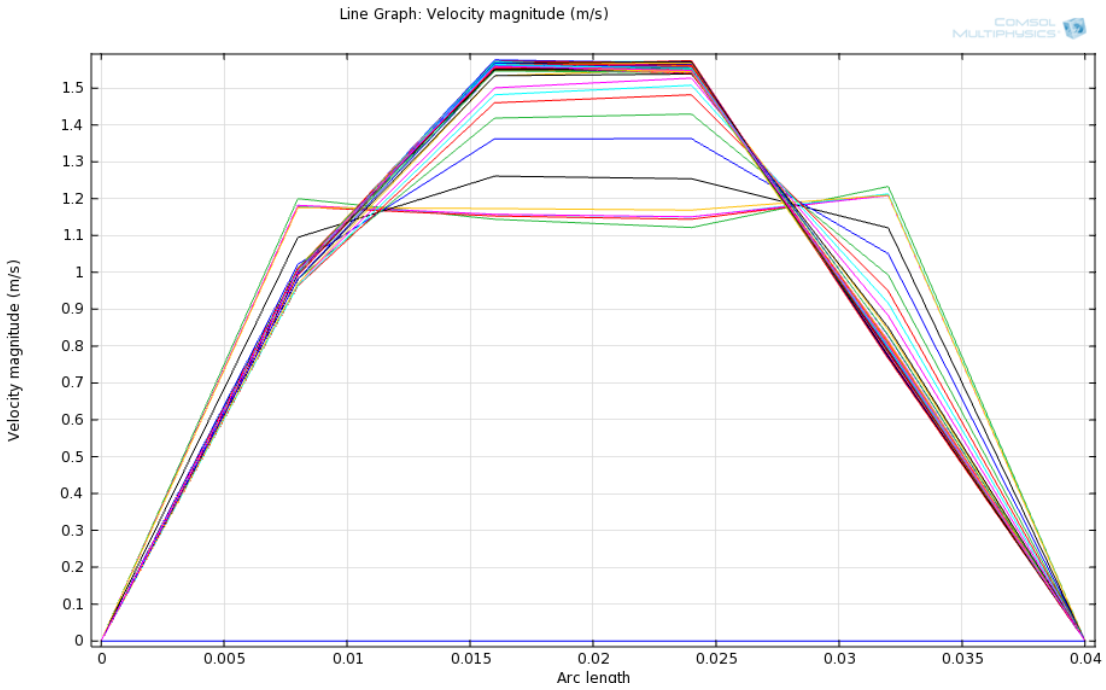

Figure 22. Velocity Profile Variations in a Finned Pipe

Figures 18-21 show that before and after the u-turn the velocity profile is turbulent and that also the pressure profile has fluctuations. So inside the finned pipe, both profiles stay un-stationary (turbulent flow conditions). Before and after the u-turn the velocity values vary between 1.3 and 1.9 m/s, and 1.3 and 1.9 m/s. Lines in Figure 22 tell that there is an eddying motion in the fluid inside the heat collection pipe. Pressure differences occur before and after the u-turn and their values vary approximately between -220 and 900 Pa.

Figure 22 shows that the modified inner structure makes the velocity profile to act more randomly and due to this, the flow behavior is more turbulent in some parts of the pipe. The *Re* was between 34 190-47 340, but it was over 10 000 only for a while. So the results from the finned-short u-pipe were slightly better than those from the smooth-short u-pipe and slightly worse than in the case of the smooth-long u-pipe. The lines in Figure 22 represent the different velocity areas in the flow.

5.4 Finned U-Pipe in 2D (Long)

The geometry and setting values of this model (Figures 23 and 24) are the same as in the previous chapter. The only difference here is the length of the pipe, 100 meters, which is a suitable length in the case of the heat collection pipes of real GSHP systems. Because of the longer pipe and the fins on the inner surface of the pipe, the modeling process took more time than the one with the short pipe. Figures 23 and 24 are zoomed on the part of the heat collection pipe which is 26 meters from the inlet channel. The Flow behavior was the same in every part of the pipe. In Figure 25 is shown how the velocity profile varies in the case of the smooth pipe.

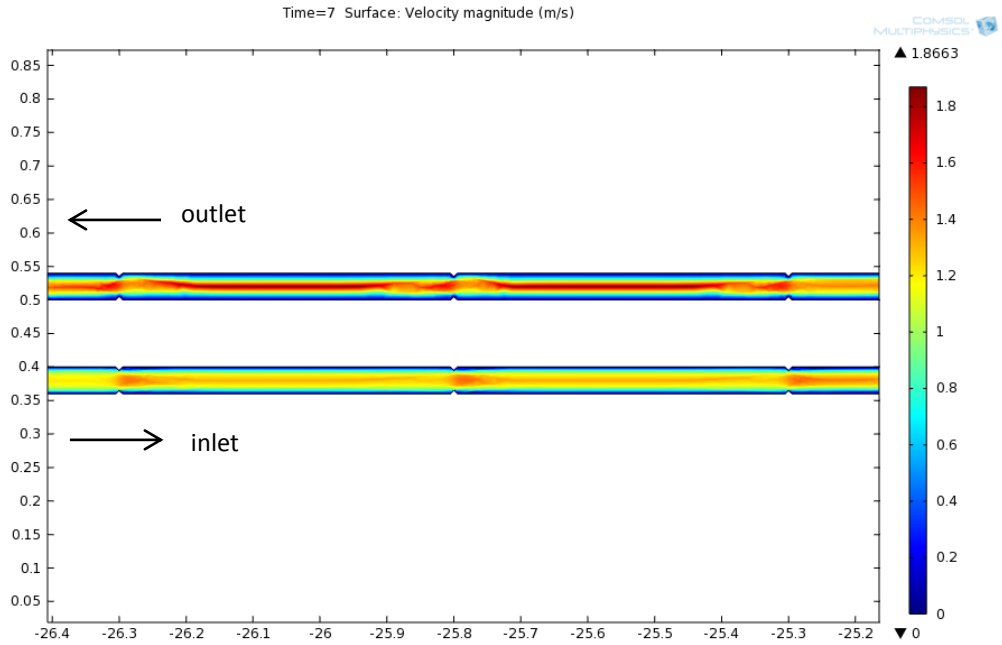

Figure 23. The Velocity Profile of a Finned-Long U-Pipe

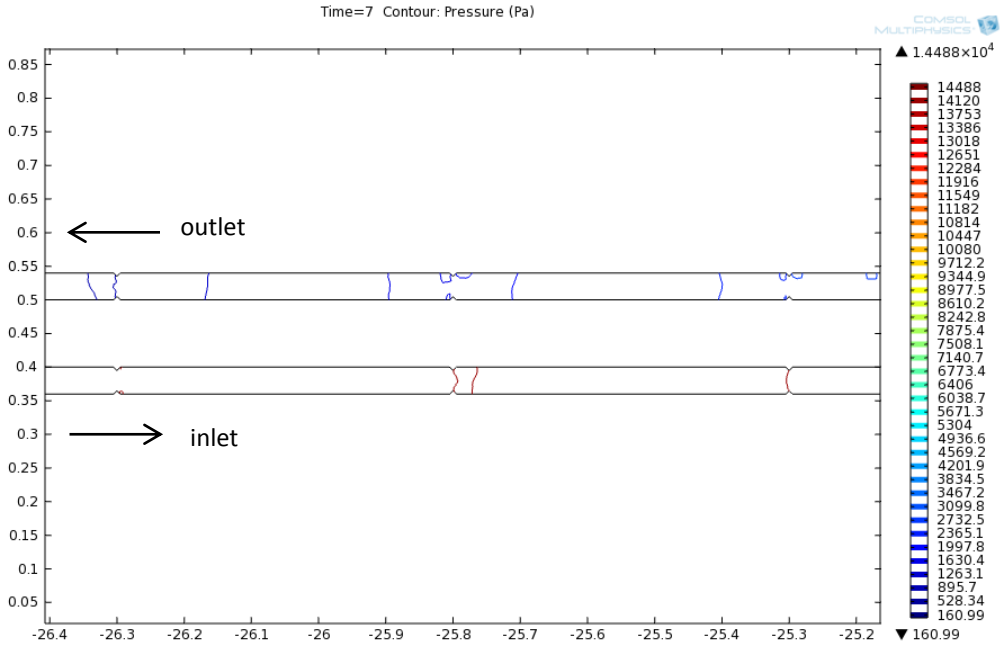

Figure 24. The Pressure Profile of a Finned-Long U-Pipe

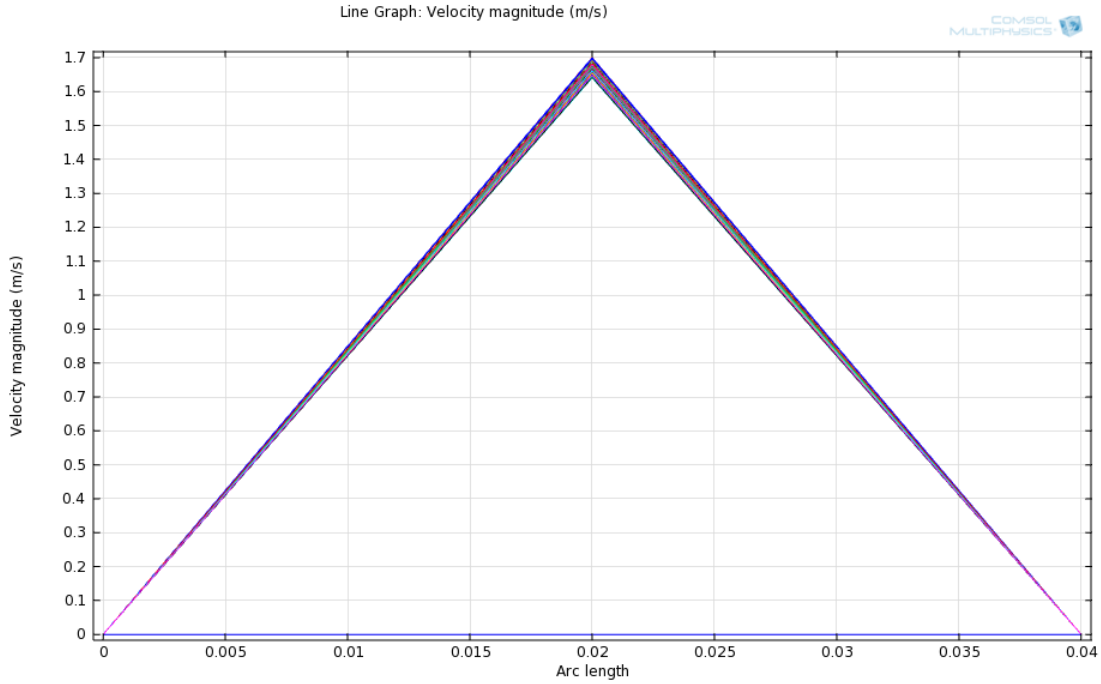

Figure 25. Velocity Profile Variations in a Long Finned Pipe

It can be noticed from Figures 23 and 24 that the velocity is rather turbulent the whole way before and after the u-turn. The pressure differences vary as well. This results in turbulent flow behavior. Eddies in the flow cause turbulent flow behavior and more properly mixed temperature areas. Before the u-turn the velocity profile varies between 1.2 and 1.4 m/s, and after the u-turn between 1.4 to 1.8 m/s. This variation causes velocity fluctuations and due to this slightly more turbulent flow behavior after the u-turn. The pressure differences occur on both sides of the u-turn and their values vary approximately between 161 Pa and 14.5 kPa. In Figure 25 the *Re* is between 31 560-47 340 and in every part of the pipe it is above 10 000. So in the case of an axial-finned pipe, the turbulence is rather major. The lines in Figure 25 represent different velocity areas in the flow.

5.5 Example of a Flow Model in a Wide Heat Collection Pipe

Here is shown how fluid flow behaves in a pipe ten times wider in diameter than the previous ones. The pipes are smooth (Figures 26 and 27) and axial finned (Figures 28 and 29) heat collection pipes. This example is made only to show more clearly how the inner profile modifications of a pipe change the flow behavior (velocities).

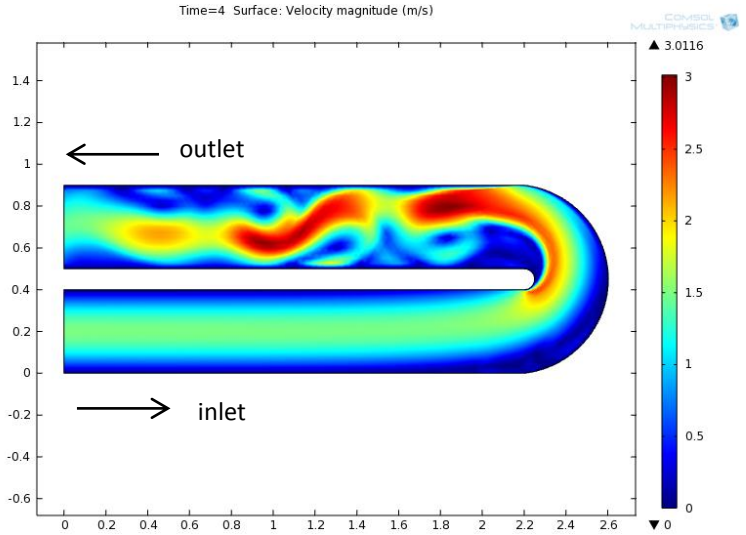

Figure 26. The Velocity Profile of a Smooth U-Pipe

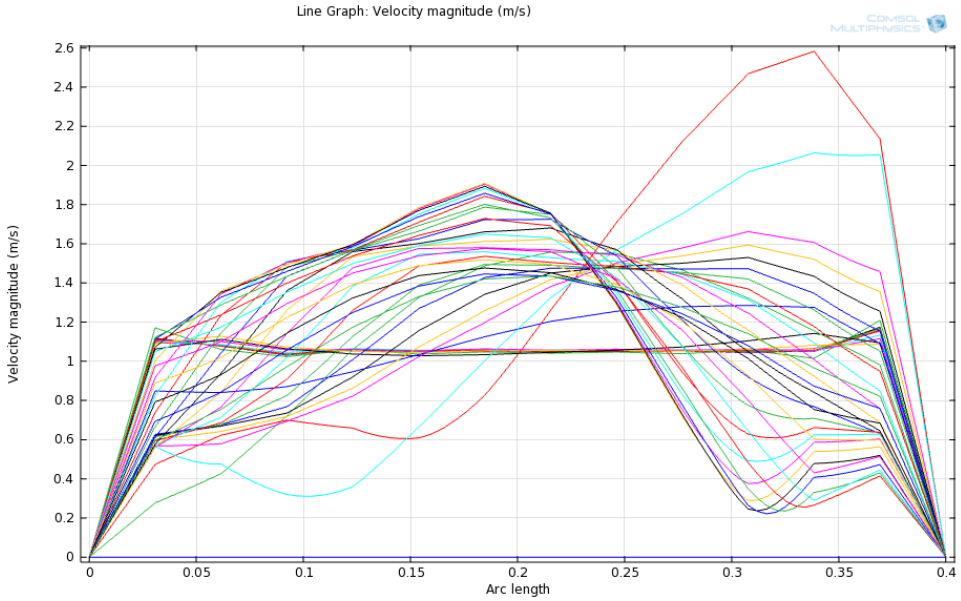

Figure 27. Velocity Profile Variations in a Smooth Pipe

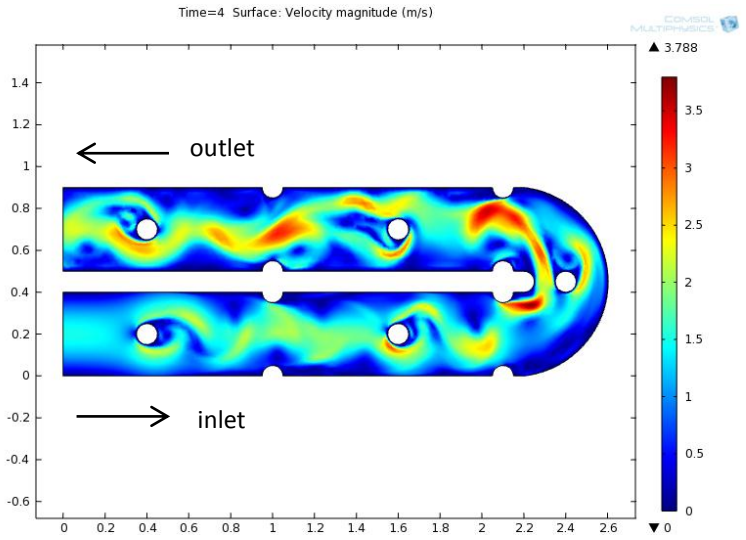

Figure 28. The Velocity Profile of a Finned U-Pipe

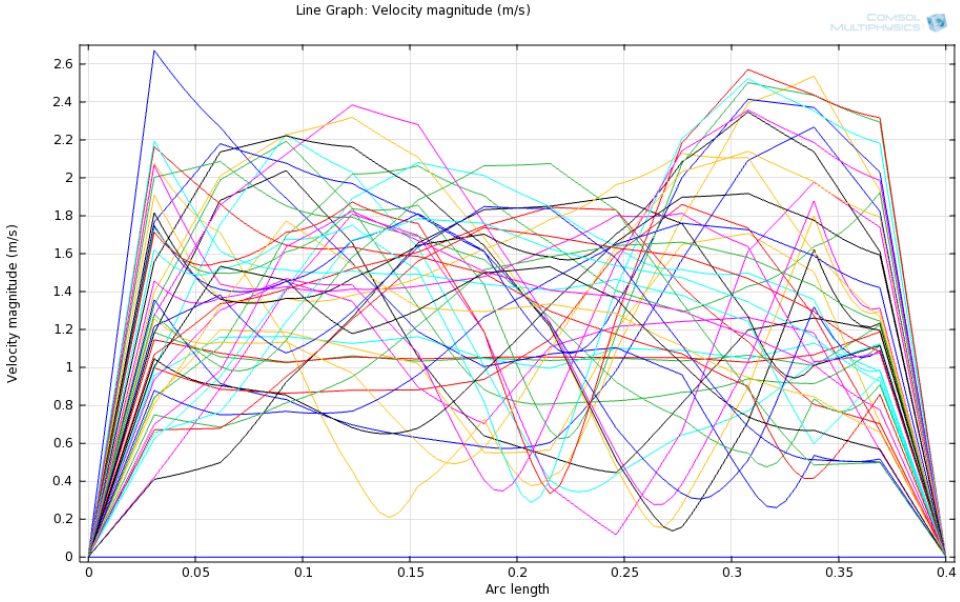

Figure 29. Velocity Profile Variations in a Finned Pipe

From Figures 28 and 29 it can be noticed that a finned pipe profile (axially finned and small finns in the middle of the pipe) changes the flow behavior to more turbulent. This phenomenon was not seen so clearly in the case of a pipe ten times narrower.

5.6 A Twisted Tape inside a Smooth Pipe in 3D

Here was examined flow behavior and pressure difference's fluctuations (stationary condition) inside a smooth pipe where a twisted tape is placed in the middle of the pipe (Figure 30). The Geometry of the twisted tape was taken from the COMSOL Multiphysics model library, which made it easier to build up the whole geometry of this model. The geometry of the twisted tape has been divided into three different parts, and these parts have been located asymmetrically towards each other (Figure 30). Physics, materials, inlet and outlet parameters etc. are modified for the requirements of this thesis. The length of the pipe, diameter, and inlet flow velocity were 42 mm; 3 mm; 50 mm/s accordingly. The inlet velocity followed the shape of the elliptical paraboloid (Function 2) (COMSOL Multiphysics 2011).

$$2 * (1 - (x\text{^}2 + y\text{^}2)/R\text{^}2) * U\_mean \qquad (2)$$

The length and the diameter of the pipe as well as the flow velocity of the inlet fluid were approximately ten to twenty times smaller than in a normal-sized heat collection pipe of a GSHP. The reason for this was a significantly faster computing time. However, it was proven that this model worked despite the fact that ten times smaller values was used. When solving the *Re*, there was taken into account the fact that ten to twenty times smaller values was used.

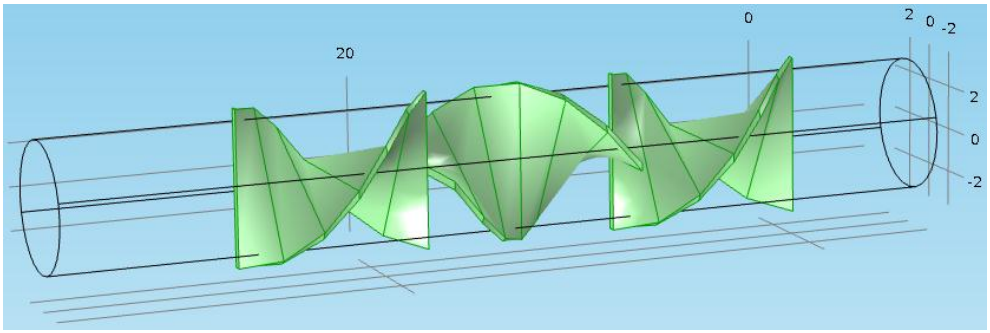

Figure 30. A Twisted Tape inside a Smooth Pipe

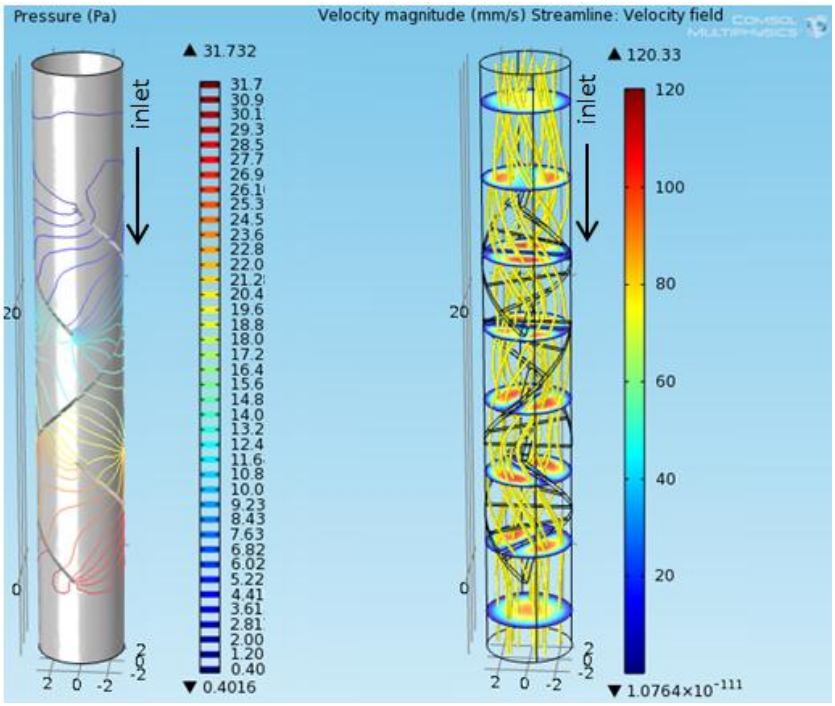

Figure 31. Velocity and Pressure Profiles in a Pipe with Twisted Tape Inserts

From Figure 31 it can be seen that the velocity varied from 70 mm/s to 120 mm/s. Pressure varied between 0.4 Pa to 31.7 Pa. The Velocity and pressure profiles in Figure 31 show that twisted tape inside the heat collection pipe makes the flow more turbulent. Relating these values to the real GSHP system values, it can be noticed that in Figure 31 the *Re* varied between 13 800 – 23 700. In every part of the twisted tape, the *Re* was over 10 000.

5.7 Twisted Tape inside a Smooth U-Pipe in 3D

Here was examined how the flow behaves when a twisted tape is placed inside a u-pipe (Figure 32) instead of a straight pipe. If the twisted tape is located only on the other side of the u-turn, it does not have such a great effect on the flow behavior after the u-turn (Figure 33). Due to this, the flow velocity and the pressure fluctuations will not be so great after the u-turn. The length, diameter and inlet flow velocity of the pipe are 42 mm; 3 mm; 50 mm/s accordingly.

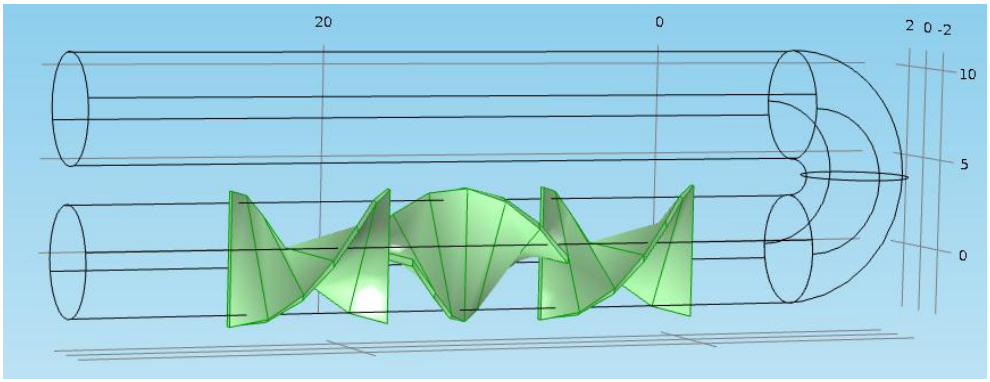

Figure 32. A Twisted Tape inside a Smooth U-Pipe

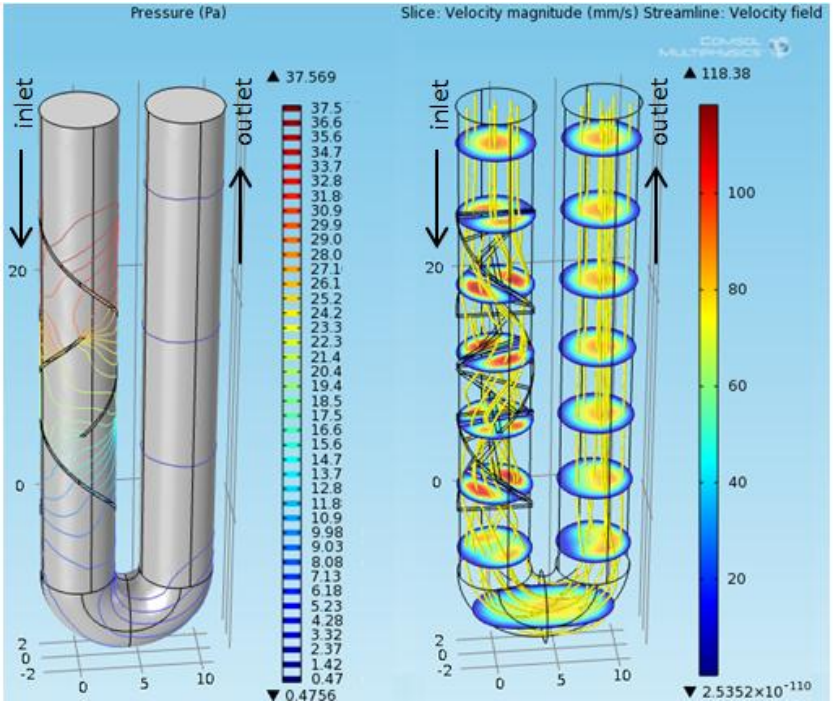

Figure 33. Velocity and Pressure Profiles in a U-Pipe with Twisted Tape Inserts

Figure 33 shows the same issues what were shown in Figure 31: that the velocity varied from 70 mm/s to 120 mm/s. Pressure varied between 0.4 Pa to 37.5 Pa. The velocity and pressure profiles in Figure 33 also show, that twisted tape inside the heat collection pipe makes the flow to act more randomly and due to this more turbulent. The Reynolds number varied between 13 800 – 23 700 (the same range as in Figure 31). After the u-turn the flow profile was smoother and more laminar than before the u-turn.

5.8 Approximation of Pressure drop and Pumping Power Variations

Here is shown how the pressure drop and pumping power values change when different pipe profiles and different inner pipe profiles are used (Figure 34). The pressure drop and pumping power are presented as functions of the product of friction factor and relative roughness with *Re* as a parameter. Friction factor and relative roughness have been dealing with the product of them. Used values were taken from the velocity profile variations (Figures 17 and 25) and from Appendices 3 and 5. Pressure drop and pumping power were calculated with Equations 10 and 11.

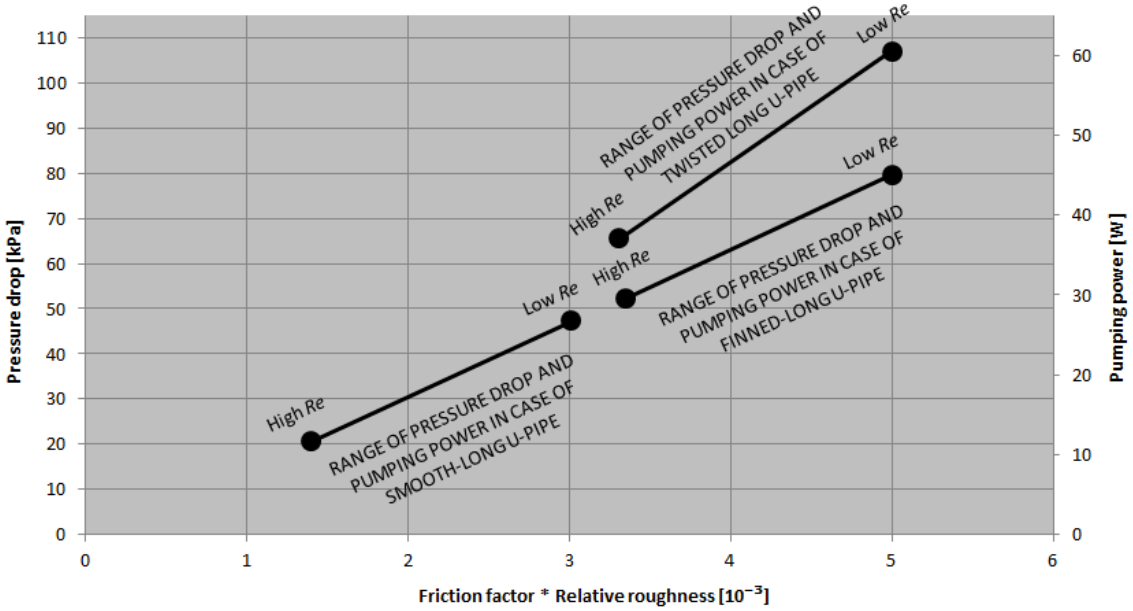

Figure 34. The Range of Pressure Drop and Pumping Power in Smooth and Finned Pipes and a Pipe where a Twisted Tape is Placed in the middle of the Pipe

Figure 34 shows that the pressure drop and the pumping power value are smallest inside the smooth heat collection pipe. The marked range area in Figure 34 presents pressure drop and pumping power values in case of low and high *Re* numbers. Low and high *Re* numbers were taken from the velocity profile variations in case of both smooth and finned heat collection pipes. Comparing the values (the Reynolds number, pressure drop and pumping power values), it can be noticed that the twisted tape modification in the middle of the heat collection pipe requires greatest amount of pumping power.

6 DISCUSSION

The modified inner structures should be used all the way in the heat collection pipes in order to guarantee as effective turbulent flow behavior and heat transfer as possible. When designing geoenergy systems and especially when designing heat collector loops (horizontal or vertical) it should be taken into account that temperature differences of the incoming and outgoing fluid flow can be three degrees (ΔT=3K) or more. So the influencing properties should meet the turbulent flow requirements of both environments, the incoming and outgoing pipe channels. In this case, one solution might be to design the inner surfaces in a different way. For example, the inner surface of the pipe's inlet could be designed to have more roughness than the inner surface of the outlet. The basic idea in this kind of a situation is to guarantee turbulent fluid flow in every circumstance and in every environment.

Few studies show the same kinds of results that came up in this thesis. An experimental study of heat transfer performance in three-dimensional internally finned steel-water heat pipe (Figure 35) was carried out by Liao Quan (Quan, Liao et al., 2006). In the study was examined heat pipes made of carbon steel, not Polyvinyl Chloride (PVC, which is the usual material for heat collection pipes in GSHP systems). All the main properties and parameters (working temperature, heat flux, inclination angle, working fluid fill ratio) that can significantly influence the heat transfer capacity and performance of the heat pipe were examined.

In Quan's study the evaporation and condensation heat transfer coefficients were found to have increased as much as 50–100 % and 100- 200 % when compared to a smooth pipe under the same conditions (Figure 36). In can be noticed that the finned structures on the inside wall of the pipe can reduce thermal resistance of the heat pipe and therefore increase the heat transfer capacity. Quan's study showed that internally finned structure inside the heat pipe has more advantages than the traditional smooth gravity-assisted heat pipe. The fluid used was water.

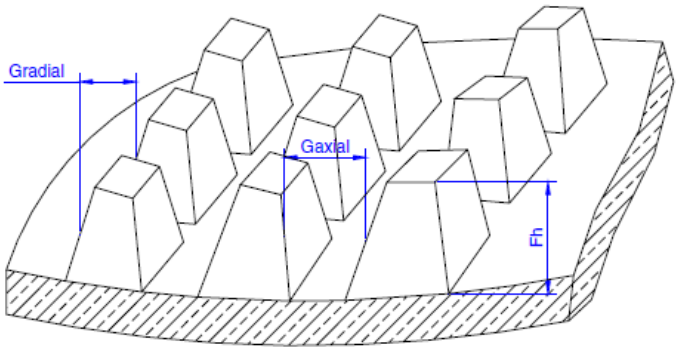

Figure 35. The Schematic of an inner fin structure (Quan, Liao et al., 2006: 1233)

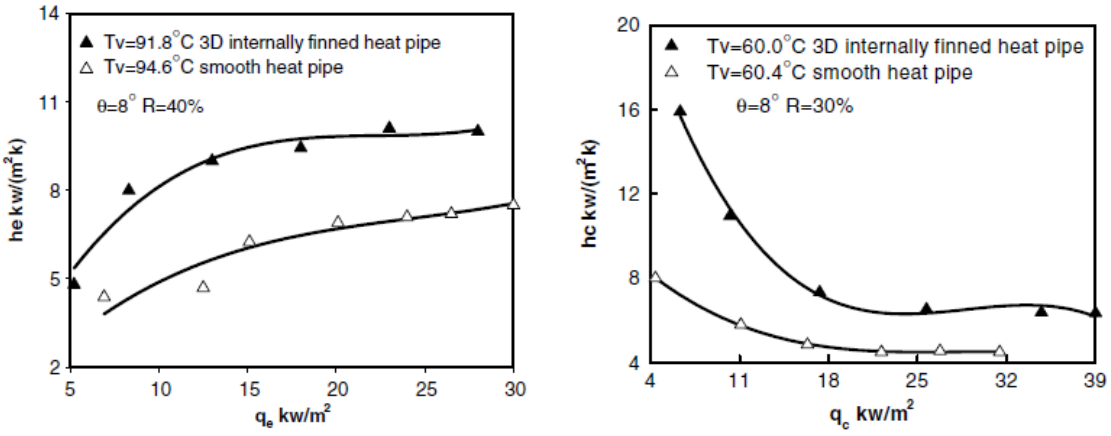

Figure 36. Evaporation (left) and Condensation (right) Heat Transfer Coefficient vs. Heat Flux (Quan, Liao et al., 2006: 1236)

Almost the same kinds of issues as in chapter 5 of this thesis were examined in the study of Eiamsa-ard Smith. (Smith, Eiamsa-ard et al., 2009) (Figure 37). In the study was examined normal twisted tape and peripherally-cut twisted tape inside heat pipes. It was noticed that when the twisted tape was peripherally-cut both the heat transfer rate and friction factor were significantly higher than in the case of a typically cut twisted tape and just plain pipe, especially in the laminar flow regime.

Higher turbulence intensity of the fluid was achieved with a peripherally-cut twisted tape than with a typically cut twisted tape and with a smooth pipe. In Figure 37, there is only two tapes examined (a peripherally-cut twisted tape and a normal twisted tape). In the study several different peripherally-cut twisted tapes are examined.

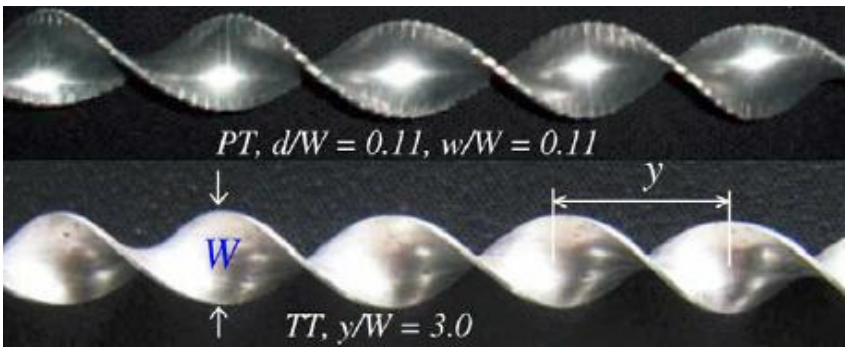

Figure 37. Geometries of a Peripherally-Cut Twisted Tape (PT) and a Typical Twisted Tape (TT) (Smith, Eiamsa-ard et al., 2009: 713)

In further research, it would be good to take the whole heat and mass transfer phenomenon into account when modeling these kinds of issues. Increasing the heat transfer effect by convection should be examined more with practical tests and measurements. Especially important would be to examine more how e.g. finned surface structures or twisted tape inside the pipe really affect the heat transfer capacity when temperature changes *in situ*.

How the *cavitation* is affecting the heat transfer capacity is an area worth further studying as well. It has to be taken into account that when there is pressure differences in the fluid in a closed environment, those pressure differences may cause cavitation. Cavitation can be compared to the transient phenomenon on power lines (electric lines). In ideal circumstances it may increase the heat transfer effect by convection, but this is rather unknown phenomenon and hard to model.

7 CONCLUSIONS

The aim of this thesis was to examine what kind of inner pipe profile ensures turbulence flow behavior in the most suitable way in the heat collection pipes of a GSHP system. The aim was to find an indicative model that could be used in the heat collection pipes of a GSHP system. Here was also examined which kind of inner profile ensures that the pumping power and pressure drop values are not too high. COMSOL models showed that with small inner surface modifications the turbulence flow behavior inside the heat collection pipes can be increased. The results showed that the modified surface structure inside the heat collection pipes (twisted tape, axial placed fins etc.) should be placed randomly in different part of the pipe (before and after the u-turn in case of a u-pipe) to guarantee turbulent flow behavior in all parts of the pipe.

Axially placed fins on the inner surface of the heat collection pipe increased the flow velocity from 29 to 50 % and the Reynolds number increased from 10 to 20 times greater. Pumping power requirements increased with 50 % compared to smooth heat collection pipe. That value was received when comparing pumping power values at points *High Re*. Although the values in case of the axially finned heat collection pipe were within rather a good range, the turbulent flow behavior was not as good as with a twisted tape inside the heat collection pipe.

The modified surface structure in the middle of the heat collection pipe gives the best results in turbulence flow behavior and at the same time keeps the pumping power and pressure drop values within a suitable range. In the optimum case a twisted modified structure in the middle of the heat collection pipe can increase the flow velocity from 50% to 65% and the Reynolds Number can be increased from 10 to 30 times greater. These are the factors that make the turbulent flow behavior to increase significantly. The pumping power requirements increased 75% compared with a smooth heat collection pipe and a heat collection pipe with twisted tape in the middle of the pipe. That value was received when comparing pumping power values at points *High Re*. Still, the pumping power requirement was rather minor. The twisted tape structure should be as thin as possible, but at the same time as twisted and as rough as possible.

Despite the fact that pumping power requirement increased as much as 75% (in case of twisted tape in the middle of the pipe), the total kilowatt hour cost was still rather minor. Approximation for the kilowatt hour cost per year was: 30,66 €/a ($10\frac{\text{cent}}{\text{kWh}} * 8760\ \text{h} * 0{,}035\ \text{kW}$). In case of smooth heat collection pipe, approximation for the kilowatt hour cost per year was: 17,52 € ($10\frac{\text{cent}}{\text{kWh}} * 8760\ \text{h} * 0{,}020\ \text{kW}$). So, the difference is still 75%, but just taking into account the amount of costs per year, it is not so major issue.

8 SUMMARY

The aim of this thesis was to outline how fluid needs to flow inside a pipe to achieve heat transfer as effective as possible. Here was also done approximation about how pressure drop and pumping power vary when the inner profile of the heat collection pipe changes. The aim of this thesis was not to design a completely new pipe profile or to get outstanding results, because the topic and results of this thesis are already well known e.g. from the heat recovery systems, where twisted inner structures inside the pipe are used. The aim of this thesis was to demonstrate how turbulent flow behavior in the heat collection pipes of a GSHP system can be achieved. This kind of solution is not used in the heat collection pipes of GSHP systems, and that is rather strange. Temperatures inside the ground and the heat collection pipes are rather low (4 – 12 ºC), so turbulent flow behavior, functionality, and the heat transfer effect of the GSHP system are very sensitive to just few degrees temperature variations.

In the beginning of this thesis the basics of the fluid dynamics were reviewed, as well as the basics of the computational fluid dynamics and different methods used. The largest focus in this thesis was on the modeling phase. Modeling was carried out with the finite element method based COMSOL Multiphysics software. The models that were built in this thesis were meant to be mainly indicative. The COMSOL models showed that a small inner surface modification increases turbulence inside heat collection pipes. The modeling was done in order to see the flow behavior of the fluid, not in order to examine the heat transfer behavior.

The results of this thesis showed that a twisted tape in the middle of a heat collection pipe is the most suitable modification to be made in order to turn the fluid flow from laminar to turbulent. Although the pumping power needs to be increased 75% from the pumping power used in a smooth heat collection pipe, the total pumping power requirement is still rather minor.

LIST OF REFERENCES

Acuña, José (2010). *Improvements of U-pipe Borehole Heat Exchangers*. Licentiate Thesis. Division of Applied Thermodynamics and Refrigeration, KTH Royal Institute of Technology, Stockholm, Sweden.

Altia Corporation (2011). *Technical data of ethanol and water mixtures*. [online] [cited 10.10.2011] Available from internet <URL: // http://www.altiacorporation.fi/fi/Tuotanto/Tekniset+etanolit/Tuotteet/

Çengel, Yunus, A., (2003). *Heat Transfer: A Practical Approach*. 2th ed. McGraw-Hill. New York, USA. ISBN: 0-07-245893-3.

Computational Fluid Dynamics (2011). [online] [cited 4.1.2012] Available from internet <URL: // http://en.wikipedia.org/wiki/Computational_fluid_dynamics

COMSOL Multiphysics – software, Help, Documentation (2011). *Reynolds Average Navier Stokes Equations*.

COMSOL Multiphysics (2011). [online] [cited 7.12.2011] Available from internet <URL: // http://www.comsol.com/products/multiphysics/

Dimplex (2008). *Planning and Installation Guide, heat pumps for space heating and domestic water heating*. [online] [cited 21.9.2011] Available from internet <URL: // http://www.dimplex.de/

Finnish Heat Pump Association, (2010). *The use of primary energy produced by ground heat pumps*. [online] [cited 9.9.2011] Available from internet <URL: // http://www.sulpu.fi

Finite Difference Method (2011). [cited 20.12.2011] Available from internet http://en.wikipedia.org/wiki/Finite_difference_method

Finite Element Method (2011). [cited 20.12.2011] Available from internet http://en.wikipedia.org/wiki/Finite_element_method

Finite Volume Method (2011). [cited 20.12.2011] Available from internet http://en.wikipedia.org/wiki/Finite_volume_method

Gehlin, Signhild (1998). *Thermal Response Test – In Situ Measurements of Thermal Properties in Hard Rock*. Licentiate Thesis. Luleå University of Technology. Sweden.

Gehlin, Signhild (2002). *Thermal Response Test – Method Development and Evaluation*. Doctoral Thesis. Division of Water Resource Engineering, Luleå University of Technology, Sweden.

Gehlin, Signhild. Nordell, Bo (1998). *Paper I: Thermal Response Test – Mobile Equipment for Determining The Thermal Resistance of Boreholes*. Division of Water Resource Engineering, Luleå University of Technology, Sweden.

Geological Survey of Finland (GTK) (2010). *Thermal Response Test*. [cited 21.9.2011] Available from internet <URL: // http://en.gtk.fi/research2/program/energy/trt.html

Gupta, H. & Roy (2006). *Geothermal energy: an alternative resource for the 21st century*. Elsevier Science, Amsterdam. ISBN: 978-0444528759.

Hughes, William. F. Brighton, John. A (1999). *Schaum's Outline of Theory and Problem of FLUID DYNAMICS*. McGraw-Hill. New York, USA. ISBN: 0-07-031118-8.

Hämäläinen, Jari[1]. Järvinen, Jari[2] (2006). *Finite Element Method in Computational Fluid Dynamics*. 2th ed. [1]University of Kuopio, Finland. [2]CSCS – Swiss National Supercomputing Centre, Switzerland.

ICAX (2009). *Asphalt Solar Collector*. [cited 21.9.2011] Available from internet <URL: // http://www.icax.co.uk/asphalt_solar_collector.html

Kuzmin, Dmitri (2010). *A Guide to Numerical Methods for Transport Equations*. Friedrich-Alexander University, Erlangen-Nürnberg, Germany.

Kuzmin, Dmitri (2011). *Introduction to Computational Fluid Dynamics*. Institute of Applied Mathematics, University of Dortmund.

Leppäharju, Nina (2008). *Geophysical and geological factors in the utilization of ground heat*. Master´s Thesis. Faculty of Science, University of Oulu, Oulu, Finland.

Mateve Ltd., customer magazine, 1/2008.

Mäkelä, Mikko., Lauri Soininen, Seppo Tuomola & Juhani Öistämö (2005). *Technical Formulas: Basic Formulas of Mathematics, Physics, Chemistry and Strength of Materials, and SI System of Units*. 5th ed. Hämeenlinna: AMK-Kustannus Ltd., Tammertekniikka. ISBN: 952–5491-08-0.

Ochsner, Karl (2008). *Geothermal Heat Pumps: A guide for Planning & Installation*. London, UK: Earthscan. ISBN-13: 978-1-84407-406-8.

Petrilia, Titus[1]. Trif, Damian[1]. Brezinski, Claude[2] (*Editor of Numerical Methods and Algorithms, Volume 3*) (2005). *Basics of Fluid Mechanics and Introduction to Computational Fluid Dynamics*. [1]Babes-Bolyai University, Cluj-Napoca, Romania. [2]Université des Sciences et Technologies de Lille, France. Springer Science + Business Media, Inc. Library of Congress Cataloging-in-Publication Data. ISBN: 0-387-23838-7.

Pitkäranta, Juha (2009). *The development of groundheat with HDD technology*. Bachelor´s Thesis. Satakunta University of Applied Science, Pori, Finland.

Quan, Liao[1]. Tien-Chan, Jen[1]. Qinghua, Chen[1]. Longjian, Li[2]. Wenzhi, Cui[2] (2006). *Heat transfer performance in 3D internally finned heat pipe*. s.1231-1237. Science Direct. [1]Mechanical Engineering Department, University of Wisconsin Milwaukee, USA. [2]College of Power Engineering, Chongqing University, Chongqing, China.

Reinikainen, Pertti (2009). *Sustainable society – Annual seminar program*. Vaasa, Finland.

Saksi, Heli (2008). *Refrigerant's effect on energy efficiency of a ground source heat pump*. Master's Thesis. Tampere University of Science, Tampere, Finland.

Smith, Eiamsa-ard[1]. Panida, Seemawute[2]. Khwanchit, Wongharee[3]. (2009). *Influences of peripherally-cut twisted tape insert on heat transfer and thermal performance characteristics in laminar and turbulent tube flows*. s.711-719. Science Direct. [1]Department of Mechanical Engineering, Faculty of Engineering, Mahanakorn University of Technology, Bangkok, Thailand. [2]Department of Civil Engineering, Faculty of Engineering, Mahanakorn University of Technology, Bangkok, Thailand. [3]Department of Chemical Engineering, Faculty of Engineering, Mahanakorn University of Technology, Bangkok, Thailand.

White, Frank, M. (2008). *Fluid Mechanics*. 6th ed. McGraw-Hill. New York, USA. ISBN: 978-0-07-293844-9

Xu, Qinwu[1]. Solaimanian Mansour[2] (2009). *Modeling temperature distribution and thermal property of asphalt concrete for laboratory testing applications*. s.487-497. Science Direct. [1]Civil Architectural and Environmental Engineering, The University of Texas at Austin, USA. [2]Pennsylvanian Transportation Institute, Penn State University, USA.

Xu, Xiaowei[1]. Spitler, Jeffrey, D.[1] (2006). *Modeling of Vertical Ground Loop Heat Exchangers with Variable Convective Resistance and Thermal Mass of the Fluid*. Proceedings of the 10th International Conference on Thermal Energy Storage-Ecostock 2006, Pomona, New Jersey. [1]School of Mechanical and Aerospace Engineering, Oklahoma State University, USA.

APPENDICES

APPENDIX 1: Geoenergy Research Project

University of Vaasa

Faculty of Technology

Geoenergy Research Project

The technology used with seabed sediment heat is low-energy network technology, which was successfully introduced at the Vaasa Housing Fair in 2008. The method has been developed in Vaasa and it has raised great interest among builders.

AIMS OF RESEARCH

The aim of this research project is to utilize the heat of different stratum layers, such as seabed sediment, water system, soil, asphalt and rock, with as effective methods as possible. The purpose is to found a working research and development center, which will offer possibilities for industry to research and test the properties of heat pumps, heat collection pipes and refrigerants. The energy received is meant to be used in the properties of the neighboring campus area.

TECHNOLOGY

One of the objectives of the Geoenergy Research Project is to examine the background theories of different heat sources more closely. The technology in low-energy networks will be investigated and developed to be even more effective in both heating and cooling sectors and also in the sectors of heat recovery and heat transfer. The research project will also include methods of finance and business models for different technical solutions.

NATIONAL AND INTERNATIONAL

Vaasa Energy Institute was one of the organizers of the International energy conference held at the University of Vaasa on 9 – 11 July 2008.

"Renewable Efficient Energy. Nordic Conference on production and use of renewable energy"

The conference had over 60 participants around Europe. One of the main topics in presentations was Vaasa Housing Fair 2008 and the energy solutions used there.

Figure 1. Geoenergy park

Figure 2. Building plan of the Geoenergy park

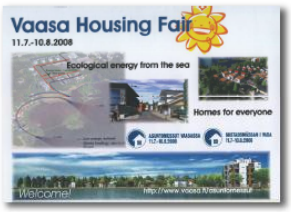

Figure 3. Vaasa Housing Fair 2008

A permanent research and development infrastructure, platform, will be executed by Vaasa Energy Institute. The project contributes to the product development of energy technology. The center is also meant to be used for multilingual education at an international level. The mobile unit enables international research and national customized research. Results will be actively released and the aim is to publish a practical guide on the utilization of seabed sediment heat.

The laboratories as well as heat distribution and heat pump centers of the Geoenergy Research Project will be located on the coastal area by the University of Vaasa. Studied and used heat sources will be located on the same area. This total concept ensures ideal, versatile circumstances for the success of the research project. Whether examined on a national or international level, the research project has good chances to become a success story from Vaasa.

Used energy solutions were: low-energy networks for seabed sediment, microturbine and biogas solutions and solid oxide fuel cells. Low-energy networks and their technology got a significant foothold in energy production on a local level and in energy self-sufficiency on a national level.

The second *REEN* Conference will take place in March 2012 in co-operation with EnergyVaasa.

Research Manager Erkki Hiltunen, erkki.hiltunen@uwasa.fi, +358 (0)50 590 8803
Project Researcher Antti Savola, antti.savola@uwasa.fi, +358 (0)44 024 4528

Faculty of Technology / Energy technology and Physics, University of Vaasa, Vaasa Energy Institute, Finland
www.uwasa.fi, www.vei.fi, P. O. Box 700, FIN-65101 Vaasa, Finland, Yliopistonranta 10

Vaasa Energy Institute = UNIVERSITY of VAASA + NOVIA + VAASAN AMMATTIKORKEAKOULU VASA YRKESHÖGSKOLA UNIVERSITY OF APPLIED SCIENCES

APPENDIX 2: Heat Equation

According to the first law of thermodynamics (**X**) and law of heat conduction → *Fourier's first law* (**X1**), the temperature difference changes on the object's internal energy and the heat flux density depends on heat conductivity and temperature gradient.

$$\Delta U = c_{\mathrm{p}} m \Delta T \text{ (“}\textit{heat flow in a solid}\text{”} \rightarrow C\Delta T) \quad \textbf{(X)}$$

$$q'' = -\lambda \frac{\partial T}{\partial x} \quad \textbf{(X1)}$$

Fourier's second law leads to **X2**.

$$-\boldsymbol{\nabla} \cdot \boldsymbol{q}'' = \rho c_{\mathrm{v}} \frac{\partial T}{\partial t} \quad \textbf{(X2)}$$

Placing **X1** on the **X2** is obtained **X3**.

$$\frac{\partial T}{\partial t} = \frac{\lambda}{\rho c_{\mathrm{v}}} \nabla^2 T \quad \textbf{(X3)}$$

Placing **X3** on the **X**6 is obtained **X7**. **X5** is cartesian coordinate expression, **X6** is cylindrical coordinate expression (Mäkelä et al., 2005).

$$\boldsymbol{\nabla} = \frac{\partial}{\partial x}\boldsymbol{e}_x + \frac{\partial}{\partial y}\boldsymbol{e}_y + \frac{\partial}{\partial z}\boldsymbol{e}_z \quad \textbf{(X4)}$$

$$\nabla^2 = \boldsymbol{\nabla} \cdot \boldsymbol{\nabla} = \frac{\partial^2}{\partial x^2} + \frac{\partial^2}{\partial y^2} + \frac{\partial^2}{\partial z^2} \quad \textbf{(X5)}$$

$$\nabla^2 = \boldsymbol{\nabla} \cdot \boldsymbol{\nabla} = \frac{1}{r}\frac{\partial}{\partial r}\left(r\frac{\partial}{\partial r}\right) + \frac{1}{r^2}\frac{\partial}{\partial \phi}\left(\frac{\partial}{\partial \phi}\right) + \frac{\partial}{\partial z}\left(\frac{\partial}{\partial z}\right) \quad \textbf{(X6)}$$

$$\overbrace{\frac{\partial T}{\partial t} = \frac{1}{r}\frac{\partial T}{\partial r}\left(\frac{\lambda}{\rho c_{\mathrm{v}}} r \frac{\partial T}{\partial r}\right) + \frac{1}{r^2}\frac{\partial T}{\partial \phi}\left(\frac{\lambda}{\rho c_{\mathrm{v}}}\frac{\partial T}{\partial \phi}\right) + \frac{\partial T}{\partial z}\left(\frac{\lambda}{\rho c_{\mathrm{v}}}\frac{\partial T}{\partial z}\right)}^{Heat\ Equation} \quad \textbf{(X7)}$$

Where, $\frac{\partial}{\partial x}$ is partial derivate and $\frac{\partial^2}{\partial x^2}$ is second order partial derivative.

APPENDIX 3: Moody Diagram

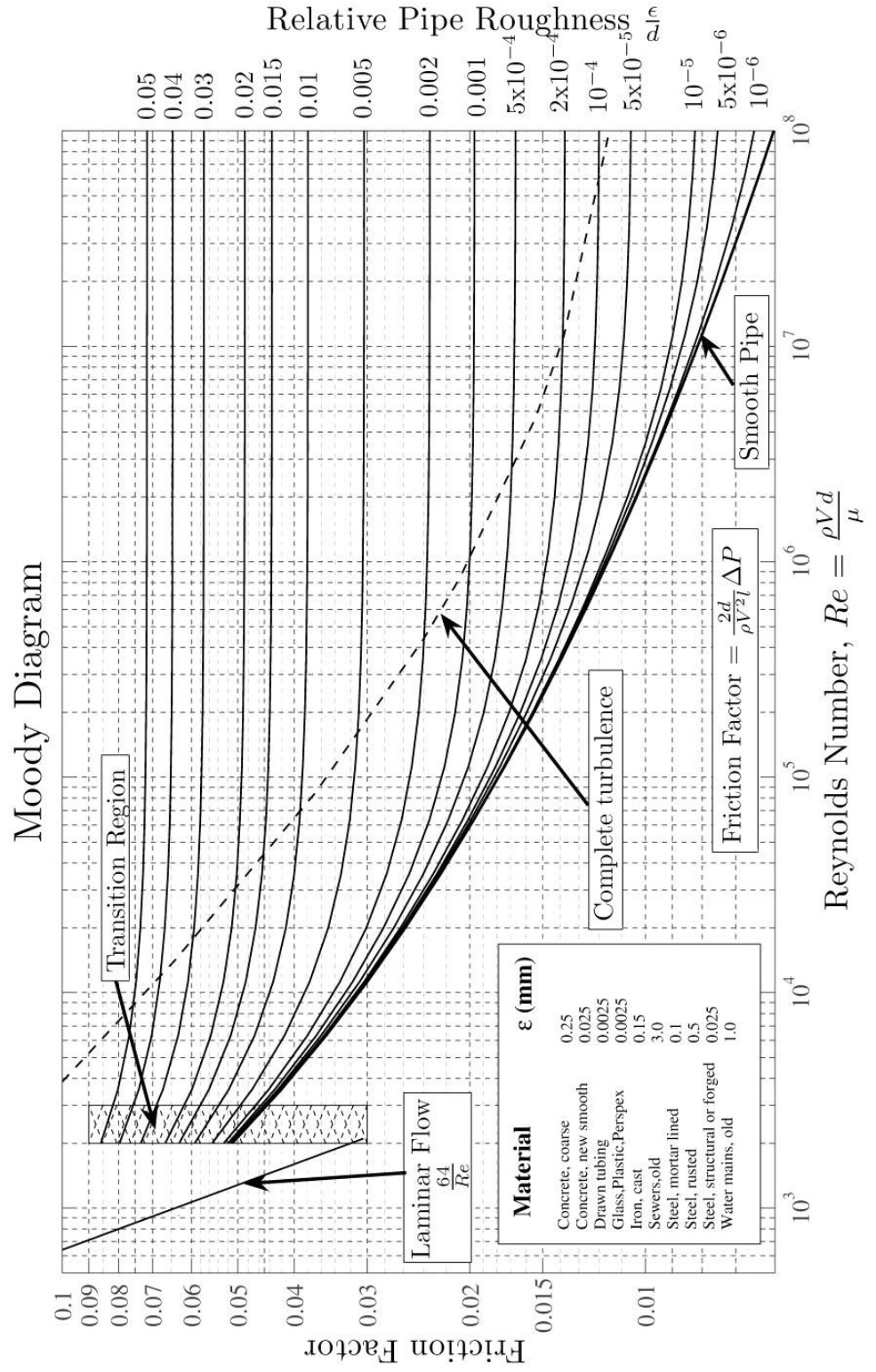

Moody diagram (Çengel 2003)

APPENDIX 4: Mean Velocity and Mean Temperature

The mean velocity varies in density and temperature and the value of it can be determined with the mass principle (Equation **X8**).

$$\dot{m} = \rho \mathcal{V}_{\mathrm{m}} A_{\mathrm{c}} = \int_{A_{\mathrm{c}}} \rho \mathcal{V}(r,x)\mathrm{d}A_{\mathrm{c}} \qquad \textbf{(X8)}$$

The mean velocity for incompressible flow in a circular pipe of radius R can be expressed with Equation **X9**.

$$\mathcal{V}_{\mathrm{m}} = \frac{\int_{A_{\mathrm{c}}} \rho \mathcal{V}(r,x)\mathrm{d}A_{\mathrm{c}}}{\rho A_{\mathrm{c}}} = \frac{\int_0^R \rho \mathcal{V}(r,x) 2\pi r dr}{\rho \pi R^2} = \frac{2}{R^2}\int_0^R \mathcal{V}(r,x) r \mathrm{d}r \qquad \textbf{(X9)}$$

The mean temperature ($\mathcal{T}_{\mathrm{m}}$) can be determined from the energy principle with Equation **X10**. (Çengel 2003)

$$\Phi_{\mathrm{fluid}} = \dot{m} C T_{\mathrm{m}} = \int_{\dot{m}} \rho C T_{\mathrm{m}} \mathrm{d}\dot{m} = \int_{A_{\mathrm{c}}} \rho C T_{\mathrm{m}} \mathrm{d}A_{\mathrm{c}} \qquad \textbf{(X10)}$$

With the same assumptions as with the mean velocity, the mean temperature is (Equation **X11**).

$$\mathcal{T}_{\mathrm{m}} = \frac{\int_{\dot{m}} C T_{\mathrm{m}} \mathrm{d}\dot{m}}{\dot{m} C} = \frac{\int_0^R C T_{\mathrm{m}} \rho \mathcal{V}(r,x) 2\pi r dr}{\rho C \mathcal{V}_{\mathrm{m}} \pi R^2} = \frac{2}{\mathcal{V}_{\mathrm{m}} R^2}\int_0^R \mathcal{V}(r,x) T(r,x) r \mathrm{d}r \qquad \textbf{(X11)}$$

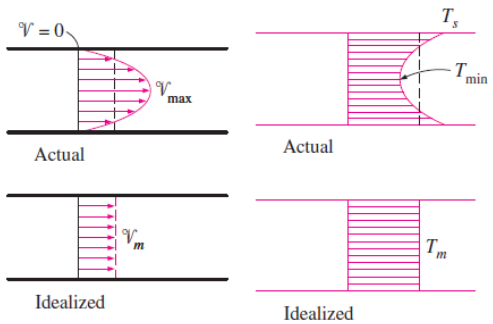

Velocity and temperature profiles (Çengel 2003: 421)

APPENDIX 5: Densities and Viscosities of Ethanol-Water Mixtures

ETANOLI- VESISEOSTEN TIHEYS JA VISKOSITEETTI

Lämpötila	Tiheys kg/m3				Viskositeetti cP			
C°	p-% 50	p-% 40	p-% 30	p-% 20	p-% 50	p-% 40	p-% 30	p-% 20
-30					4,33	4,41	4,48	4,54
-20	943,76	962,52	974,91		3,11	3,14	3,16	3,19
-10	936,56	956,06	970,32	977,64	2,30	2,30	2,31	2,31
0	929,17	949,34	965,24	975,57	1,74	1,74	1,73	1,73
10	921,59	942,38	959,73	972,52	1,35	1,34	1,34	1,33
20	913,77	935,15	953,78	968,61	1,07	1,06	1,05	1,00
30	905,71	927,64	947,37	963,91	0,87	0,86	0,80	0,84

Altia Corporation (2011).

Viscosities on the above table are dynamic viscosities. Kinematic viscosities that have been used in Figure 4 and 5 can be calculated in the following way (in the example below marked values are used from the table above):

$$\nu = \frac{\mu}{\rho} = \frac{2{,}31 * 10^{-3}\,\text{Pa s}}{977{,}64\,\frac{\text{kg}}{\text{m}^3}} \approx 0{,}00236 * 10^{-3}\frac{\text{m}^2}{\text{s}}$$

$$[1\ \text{cP} = 1\ \text{mPa s} = 0{,}001\ \text{Pa s}]$$

The Reynolds Number that was used in Figures 4 and 5 were calculated in the following way (flow rate and diameter values were from Mauri Lieskoski):

$$Re = \frac{\dot{V} D}{\nu A_c} = \frac{0{,}0006\frac{\text{m}^3}{\text{s}} * 0{,}04\ \text{m}}{0{,}00236 * 10^{-3}\frac{\text{m}^2}{\text{s}} * \pi * (\frac{0{,}04}{2})^2} \approx 8100$$